

Radical Anion Functionalization of Two-Dimensional Materials as a Means of Engineering Simultaneously High Electronic and Ionic Conductivity Solids

Károly Németh*

*Physics Department, Illinois Institute of Technology,
Chicago, Illinois 60616, USA*

A radical anion based functionalization of the basal plane of hexagonal boron nitride (h-BN) and other two-dimensional (2D) materials is proposed in the present study. The resulting materials can reversibly be oxidized without the detachment of the functional groups from the basal plane and can thus serve as surface-intercalation type cathode electroactive species and fast solid ion conductors at the same time. The functionalization of h-BN with $[\cdot\text{OBX}_3]^-$ radical anions ($\text{X}=\text{F}, \text{Cl}$) in the presence of Li, Na or Mg cations provides one example of such systems. This material can be realized in a proposed simple, two step synthesis. In the first step, a symmetric Lewis adduct of the corresponding Li, Na or Mg peroxides is formed with BX_3 . In the second step, the anion of the Lewis adduct is thermally split into two identical $[\cdot\text{OBX}_3]^-$ radical anions that covalently functionalize the B atoms of h-BN. In the maximum density surface packing functionalization, the product of the synthesis is $\text{A}_n[(\text{BN})_2\text{OBX}_3]$ ($\text{A}=\text{Li}, \text{Na}$ with $n=1$ or $\text{A}=\text{Mg}$ with $n=0.5$). In the highly oxidized states ($0 \leq n \leq 1$ for Li and Na and $0 \leq n \leq 0.5$ for Mg), the electronic conductivity of this material is in the order of 1 S/cm, similar to carbon black. In the fully reduced states ($n=2$ for Li and Na and $n=1$ for Mg), the material becomes an insulator, like h-BN. The tunability of the electronic properties of $\text{A}_n[(\text{BN})_2\text{OBX}_3]$ via the cation concentration allows for its application as multifunctional material in energy storage devices, simultaneously serving as cathode active species, solid electrolyte, electroconductive additive, separator, heat conductor and coating for metal anodes that enables dendrite-free plating. This multifunctionality reduces the number of phases needed in an all-solid-state battery or supercapacitor and thus reduces the interfacial impedance making energy storage devices more efficient. For example, $\text{Li}[(\text{BN})_2\text{OBF}_3]$ is predicted to have 5.6 V open circuit voltage vs Li metal anode, capacity of 191 mAh/g, specific energy of 1067 Wh/kg and can store energy at a (materials only) cost of 24 USD/kWh.

INTRODUCTION

The quest for high performance electrochemical energy storage devices poses a multi-objective optimization problem over the space of readily available and potentially synthesizable designer materials. The objectives include high energy and power density, safety of operation, economic and environmentally friendly composition, rechargeability, fast charging and discharging, a long cycle-life (i.e. large number of charge/discharge cycles at a steady performance) and reliable functioning in a broad temperature window.

Two-dimensional (2D) layered materials represent an attractive platform for developing effective rechargeable intercalation cathodes for these objectives as they allow for the reversible intercalation of Li^+ ions between the layers. This principle was first demonstrated on TiS_2 [1] while a more practical approach using Li_xCoO_2 ($0 < x < 1$) was developed at the same time [2, 3]. Since then, variants of Li_xCoO_2 where Co is partially substituted by Ni, Mn and Al have also been developed to mitigate the scarcity of cobalt [4–7].

On the anode side, graphite, another 2D layered material, and similar carbonaceous materials containing layered fused aromatic rings (such as coke) were proposed and successfully applied as Li-intercalation systems [8, 9].

Electrode materials can be divided into two groups: in-

tercalation based ones (such as the LiCoO_2 cathode and the graphite anode) and conversion based ones (such as the sulfur cathode [10, 11] and the silicon anode [12]). Whenever possible, intercalation based electrodes appear more attractive as they typically have much smaller volume changes than conversion ones during the cycling of the battery. Intercalation based electrodes also have a more steady chemical structure as compared to conversion based ones. Chemical bonds in the latter ones may go through radical transformation during cycling.

The present paper is highly interdisciplinary as it combines fields of theoretical materials design, quantum chemical prediction of properties, synthesis design, thermal stability analysis, electrochemistry and economic analysis. Therefore, it is important to discuss its layout and logic first, before the elaboration starts.

First, a thorough review is provided about past and present attempts to achieve the objectives mentioned at the beginning of the present Introduction. Particular attention is given to designer strategies on how simultaneous high energy and high power density batteries might be realized. This review describes the historical roots and emergence of the graphene oxide (GO) battery as the sole existing demonstration of high energy and high power energy storage at the same time.

We will point out that the great performance of the GO battery is conditional to the presence of a Lewis

acid donating electrolyte and this Lewis acid forms Lewis adduct with GO. A particularly important Lewis acid is boron trifluoride (BF_3) donated by $(\text{Li}/\text{Na})\text{BF}_4$ electrolyte. The Lewis adduct involves various forms of the $-\text{OBF}_3$ functional group that plays a key role in the present study. The review also discusses fundamental problems of the GO problem, especially its safety problem attributed to explosive decomposition of GO upon heating.

At this point, a reference will be made to our former works [13–16] in which we proposed to substitute GO with functionalized hexagonal boron nitride (h-BN) in order to cure the thermal stability problem of GO. In addition, we have predicted that the $-\text{OBF}_3$ functionalization of h-BN would be particularly advantageous for an efficient, h-BN-based battery. This makes the key importance of the $-\text{OBF}_3$ functional group very clear, in both GO and h-BN-based batteries.

A question naturally emerges about whether such an $-\text{OBF}_3$ functionalization of h-BN is possible at all. We answer this question first by reviewing the literature for analogous functionalized h-BN. It turns out that the historically first functionalized h-BN was actually very similar: it contained $-\text{OSO}_2\text{F}$ functional groups on the surface of h-BN, covalently bound to the B atoms. This material has been synthesized first in 1978 [17] and its electrical conductivity was measured and found to be surprisingly high, 1.5 S/cm [18], especially compared to the near 6 eV band gap and insulator nature of h-BN. The $-\text{OSO}_2\text{F}$ functional groups can cover the surface of a h-BN monolayer with very high density leading to every second B atom functionalized in $(\text{BN})_2\text{OSO}_2\text{F}$.

Unfortunately, $(\text{BN})_2\text{OSO}_2\text{F}$ is not stable when in contact with base metals. It decomposes irreversibly due to the evolution of volatile molecules. Therefore, $(\text{BN})_2\text{OSO}_2\text{F}$ cannot be used directly in batteries. However, the synthesis of $(\text{BN})_2\text{OSO}_2\text{F}$ provides a great model for the synthesis of our proposed $-\text{OBF}_3$ functionalized h-BN, which has the formula of $(\text{BN})_2\text{OBF}_3$ in the most dense surface packing.

At this point, we calculate and analyze the electronic structure of the compounds mentioned so far, i.e. h-BN, $(\text{BN})_2\text{OSO}_2\text{F}$ and $(\text{BN})_2\text{OBF}_3$ as well as the reduced versions of $(\text{BN})_2\text{OBF}_3$ that form when the $(\text{BN})_2\text{OBF}_3$ is in contact with Li, Na or Mg. Furthermore, the same analysis is also carried out for $(\text{BN})_2\text{OBCl}_3$ which contains Cl instead of F in the same structure. This analysis establishes the stability of the reduced versions of $(\text{BN})_2\text{OBF}_3$ as opposed to $(\text{BN})_2\text{OSO}_2\text{F}$. It also establishes the similarity between the band structures, electronic conductivities and magnetic properties of these materials.

Following the quantum chemical analysis, we analyze the stability and decomposition reactions of $(\text{BN})_2\text{OBF}_3$ and its reduced versions on the basis of analogy with the known decomposition of $(\text{BN})_2\text{OSO}_2\text{F}$. It turns out that $(\text{BN})_2\text{OBF}_3$ has solid decomposition products and

therefore it is much safer than GO or $(\text{BN})_2\text{OSO}_2\text{F}$.

Next, we utilize the synthesis model provided by $(\text{BN})_2\text{OSO}_2\text{F}$ and propose a similar, simple synthesis for the reduced versions of $(\text{BN})_2\text{OBF}_3$. Additionally, we also propose and analyze alternative synthesis methods.

The above are followed by a discussion of application areas of $(\text{BN})_2\text{OBF}_3$. These include cathode active species, solid electrolytes, electroconductive additives, separators and anode coatings for dendrite-free plating of Li, Na and Mg.

Finally, an economic analysis is provided for the economic viability of the proposed batteries.

DESIGN STRATEGIES FOR HIGH ENERGY AND HIGH POWER BATTERIES

Artificial intercalation systems

Artificial intercalation systems may be built by inserting “pillaring” ions or molecules between the loosely bound layers of some 2D materials thereby expanding the interlayer distances [19, 20]. The interlayer-expanded 2D materials allow for the rapid intercalation of Li^+ , but also that of larger cations, such as Na^+ , K^+ , Mg^{2+} or complex cations, such as $[\text{MgCl}]^+$ [21]. This technique greatly increases both the capacity and rate performance of electrodes based on 2D layered materials [20, 21]. Ideally, a small amount of pillaring agent is sufficient for the interlayer expansion and most of the interlayer space may be utilized for a dense packing of intercalated ions. A significant advantage of such artificial intercalation systems over naturally occurring ones is the tunability of the rate performance of the electrodes through the pillaring agents. Such artificial intercalation systems are increasingly important for beyond-Li-ion batteries, as both the number of naturally occurring minerals for Na or Mg intercalation is more limited than that of Li intercalating ones and their rate performance at room temperature (dependent on ionic conductivity) is typically low as compared to the targeted performance. Ideal intercalation systems should also provide good rate performance in a broad temperature range, starting as low as -60°C and reaching as far as at least 200°C : the lower value corresponding to harshest winter conditions and the highest values to safe operations when the environment of the battery is highly overheated due to fire, or other sources of radiating heat [22–28]. Artificial intercalation systems appear to provide an efficient solution for all the above mentioned problems.

Perhaps the oldest form of interlayer expansion of 2D materials has been discovered more than a hundred years ago, when sulfuric acid was utilized as a pillaring agent for the interlayer expansion of graphite [29], as a method that accelerates the oxidation of graphite and the formation of graphene oxide [30–34]. About forty years

ago, first stage intercalation compounds of h-BN have been synthesized by the rapid reaction of h-BN with strong oxidizer bis(fluorosulfonyl)peroxide ($\text{FO}_2\text{S-O-O-SO}_2\text{F}$), source of (fluorosulfonyl)oxy radicals ($\cdot\text{OSO}_2\text{F}$) [17, 18]. $\text{FO}_2\text{S-O-O-SO}_2\text{F}$ is a liquid at room temperature and is in equilibrium with $\cdot\text{OSO}_2\text{F}$ radicals [18]. More recently, a simple drying of concentrated H_2SO_4 , H_3PO_4 or HClO_4 over h-BN also resulted in intercalation and interlayer expansion of h-BN [35].

For the purpose of Mg^{2+} or MgCl^+ ion intercalation, interlayer expansion in transition metal containing 2D layered materials, such as in TiS_2 and MoS_2 , has been carried out electrochemically whereby the pillaring cations included imidazolium, pyridinium, ferrocenium, alkyl-ammonium, pyrrolidinium or piperidinium cations, while the corresponding anions were Cl^- , $[(\text{CF}_3\text{SO}_2)_2\text{N}]^-$, BF_4^- , or $\text{AlCl}_x\text{R}_{4-x}^-$ [19–21]. Note that the pillaring salts in the above systems are neither known to form covalent bonds with the layers of the host material nor participate in redox reactions.

Edge functionalization and the graphene oxide cathode

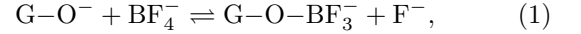
Intercalation may not only happen between two monolayers. It can also happen on the surface of a functionalized monolayer. In this case, the ions intercalate between the functional groups that are covalently bound to the monolayer. As the functionalized monolayers are open to the electrolyte on their entire surface, the rate of intercalation can be even faster than in the case of interlayer expanded layered materials. Such intercalation is an example of supercapacitor-battery hybrids or of pseudocapacitors. It is however not necessarily advantageous to exfoliate functionalized monolayers from the first stage intercalation phase, since bending and folding might occur decreasing the volumetric capacity of such systems. If the ionic conductivity of the first stage intercalation compounds is sufficient, there is no need for exfoliation.

To date, the only broadly studied example of rechargeable cathodes with functionalized 2D redox active species is based on graphene oxide (GO) [36–39]. In these studies, the reversible redox reactions are based on oxo ($=\text{O}$) groups attached to edges and defects of graphene. Oxygen atoms bound to the basal plane as epoxy groups are largely removed by gentle heating, as their reduction would cause irreversible formation of oxides. Such GO cathodes, with up to 21–32 w% oxygen content, have been successfully used with Li and Na anodes. Very high power densities of 4–45 kW/kg (on average) and specific energies of 100–500 Wh/kg have been achieved with Li anodes, and stable capacity of 300–450 mAh/g was maintained over 1000 cycles [37]. With Na anode, stable capacity at about 150 mAh/g over 300 cycles and en-

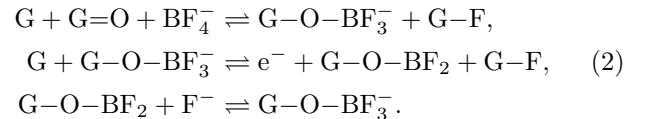
ergy densities between 100–500 Wh/kg were achieved, at power densities as high as 55 kWh/kg [38], when NaBF_4 electrolyte additive was used. With NaClO_4 additive, capacity decreased from 150 to 50 mAh/g in 300 cycles, indicating potential reactions between GO and the electrolyte additives.

While the incorporation of boron in the surface of GO was pointed out in Ref 38, its precise mechanism has not been described yet. F^- ions of BF_4^- can be exchanged to oxide ions to some extent, in the present case with oxide ions bound to the surface or edge of graphene. Similar reactions were observed for example in the reaction of hydrogen peroxide with KBF_4 [40], in the reaction of BF_3 with GO [41] or in the formation of perborates [42], also see discussion below for cyclic perborates. Furthermore, surfaces of metal oxides, such as Al_2O_3 , SiO_2 , TiO_2 , ZrO_2 , NiO , etc, are also known to irreversibly absorb BF_3 leading to the formation of (M)- OBF_2 , (M)- OB_3^- and (M)-O-(BF)-O-(M) functional groups on the surfaces of these materials, where M is a metal atom [43–46].

Based on the analogy to the reaction of GO and BF_3 in Ref 41 and that of oxidized h-BN and BF_3 as discussed in our former work [16] the likely mechanism of boron incorporation from NaBF_4 into GO may be based on the following equations in the discharged state:



where G stands for graphene and G-O^- for reduced oxygen atoms covalently bound to graphene. In the charged state or during charging, the following reactions may happen:



The above reactions are likely responsible for the steady and even somewhat increasing capacity during cycling of the GO cathodes with NaBF_4 electrolytes in Ref 38. The increasing capacity may originate from the utilization of epoxy oxygen of GO that would otherwise irreversibly form Na_2O . The conversion of edge-bound oxo groups to their Lewis adducts with BF_3 may further stabilize these units on the edge of graphene. Thus, the Lewis adducts of both epoxy and oxo groups of GO may become more stable resulting in stable capacities. It is very likely, although not noticed yet, that the use of LiPF_6 electrolyte additive leads to analogous reactions and may contribute to the cycling stability of Li-GO batteries [36, 37], as the conjugate PF_5 is a Lewis acid and can form adducts with GO. Also note that similar advantages have been seen on the performance of Li-ion batteries with Lewis adducts of BF_3 applied as electrolyte additives [47–51].

All-solid-state Li and Na ion batteries have also been built and tested where GO plays the role of cathode ac-

tive species, solid electrolyte and separator at the same time [52]. However, the capacity of this batteries quickly decreases upon cycling, likely for at least the lack of stabilizing BX_3 additives as seen for the above liquid electrolyte GO batteries.

Basal plane functionalization in h-BN cathodes and elsewhere

Another recent example of rechargeable 2D cathode actives species is based on h-BN functionalized with fluorene on its edges and defect sites [53]. Contrary to the expectation that a fluorinated h-BN would behave similarly to graphite fluoride and form a non-rechargeable battery [54], Ref. 53 demonstrates rechargeability of F-doped h-BN cathode with a Mg anode at 50 mAh/g capacity over 80 cycles. Also note that it is extremely difficult to make stable basal plane functionalized fluorinated h-BN, and to date it was only possible by a high energy ion irradiation of a LiF/h-BN/Cu heterostructure [55].

While the reversible capacity of GO cathodes is largely associated with edge and defect functionalization, the utilization of the basal plane functionalization for reversible redox processes is still to be developed and is very desirable. A close packing of the basal plane with redox active functional groups can potentially enable large capacity without the generation of edges and defect sites in the 2D material. Also note the thermal instability of GO that is the main hurdle for its industrial scale production and its limited safety in applications [56–59].

Free radicals appear to be the best and most general means for a stable covalent functionalization of the basal plane. Graphite fluoride or graphite oxide can both be considered as functionalized by fluorene or oxygen radicals. Radical functionalization of the basal plane of h-BN has been carried out with $\cdot OSO_2F$ [17, 18], $\cdot NH_2$ [60–62], $\cdot O\cdot$ and ozone [63–67], $\cdot OH$ [61, 62, 68], $\cdot SO_3H$ [62, 69–71], $\cdot R$ [72, 73] and $\cdot OR$ [68] (R being alkyl or aryl), and $\cdot CBr_2$ [74] radicals. These radicals preferentially bind to the basal plane B atoms of h-BN as its valence shell is incomplete and can in principle accept two more electrons [16].

Lewis adduct formation between the B of h-BN and the N of the amino groups of non-radical amines has also been reported [75], however it has not been conclusively established that the formation of Lewis adducts happens at the edges/defects or on the basal plane. Such Lewis adducts should preferentially form between edge or defect B atoms and amino groups as the edge atoms of h-BN clearly have strong Lewis acid/base character. Basal plane atoms of h-BN are much more difficult to bring into a non-planar hybridization necessary for Lewis adduct formation, albeit folding and bending of the h-BN sheet may increase Lewis acid/base character of some surface atoms.

Hydroxide anions covalently functionalize the edges or defect sites of h-BN, but not the basal plane, when h-BN is ball-milled and exfoliated in aqueous NaOH solution [76]. Edge functionalization of h-BN is likely dominant also in the melt phase of hydroxides [77]. The reaction of h-BN with strong Lewis base nitrides, such as Li_3N , is assumed to go through the formation of a complex with approximate composition $Li_3N \cdot 3BN$ before it results in Li_3BN_2 and cubic BN [78]. This indicates that the reaction of h-BN with very strong Lewis bases may result in a basal plane functionalized h-BN, however these complexes likely have limited thermal stability.

Recently discovered cyanographene and its derivative graphene acid are also examples of basal plane functionalized 2D materials and have been successfully tested for supercapacitor applications [79–81]. While the $-CN$ and $-COOH$ functionalizations of the basal plane of graphene allow for the binding of redox active species, such as iron oxides/oxyhydroxides [81] the $-CN$ and $-COO(H)$ groups themselves do not appear to participate in redox reactions, hence these materials in themselves can be applied only as electrodes in double layer capacitors, although they provide great improvement in capacity as compared to non-functionalized graphene [80]. Also, the density of functionalization is only about 15%, which is large for most known functionalized graphenes, but still much smaller than in fluorographene, graphene (mon)oxide, or in $(BN)_2OSO_2F$ (made of highly oriented pyrolytic h-BN) [18].

Nitrogen doped graphene also contains basal-plane bound nitrogen atoms and greatly improves the capacity of graphene supercapacitors [82]. The N atoms mostly dope the basal plane (substitute C atoms) instead of functionalizing it and participate only to a limited extent in redox reactions. All these latter systems (N-doped and $-CN$ or $-COO(H)$ functionalized graphene) need an external electrolyte, because they cannot provide solvation shells to cations due to the insufficient density of functional groups or the in-plane nature of the doping.

As an example of basal plane functionalized cathode active species, $Li[(BN)_2OBF_3]$ (discharged form) has been proposed in our previous work [13, 14, 16]. This material is closely related to the above mentioned $\cdot OSO_2F$ functionalized h-BN, however, instead of a charge-neutral radical, an anionic radical, $\cdot OBF_3^-$ functionalizes the B atoms of h-BN. The radical character of the anion ensures its covalent binding to h-BN while its negative charge enables the holding of cations between the $\cdot OBF_3^-$ groups on the surface of h-BN. Furthermore, when densely functionalized, this system also enables the solvation of cations without external electrolyte and presents a solid ion conductor.

In addition to excellent ionic conductivity, the electronic conductivity of $Li[(BN)_2OBF_3]$ is also predicted to be great, due to a high concentration of holes in the N lone pairs (p_z orbitals). These N-holes are gen-

erated by the strongly electron withdrawing character of the $\cdot\text{OBF}_3^-$ radicals that withdraw almost a whole electron charge from the two N-s per formula unit [16]. We have recently pointed out the existence and charge storage ability of similar N-hole states in Li_3BN_2 cathode active species [83]. The electronic conductivity of $\text{Li}[(\text{BN})_2\text{OBF}_3]$ is expected to be close to that of $(\text{BN})_2\text{OSO}_2\text{F}$, which was measured to be 1.5 S/cm [18]. This electronic conductivity is in the same order of magnitude with graphene (7.14 S/cm) [84, 85] and electroconductive carbon additives (2-12 S/cm) [86] typically used in batteries. The concentration of N-holes and thus the electronic conductivity of $\text{Li}_x[(\text{BN})_2\text{OBF}_3]$ depends on its oxidation state: the largest concentration of holes is in the fully oxidized state ($x=0$) and it gradually decreases as this system becomes fully reduced ($x=2$). The as synthesized state (proposed below) is at $x=1$ and corresponds to the half reduced system.

Therefore, $\text{Li}[(\text{BN})_2\text{OBF}_3]$ (and the analogous Na and Mg compounds) can potentially provide three functions of the cathode in a single material: ionic and electronic conduction and electroactive species. The combination of these features in a single material can therefore save a number of solid phases that would normally be necessary in a composite cathode and eliminates interfacial impedance on the respective phase boundaries [87].

Graphene vs h-BN for functionalization

As described in Refs 17 and 18, $\cdot\text{OSO}_2\text{F}$ functionalization of graphene has been carried out in the form of first stage intercalation complexes of graphite of $\text{C}_{8.5}\text{OSO}_2\text{F}$ stoichiometry. Functionalization of graphene with $\cdot\text{OBF}_3^-$ radical anions is also possible, however the product is expected to be much less thermally stable as volatile decomposition product carbon-monoxide is expected (besides BF_3).

The surface density of functional groups on graphene is expected to be significantly lower than in h-BN. This is indicated by the stoichiometry of $\text{C}_{8.5}\text{OSO}_2\text{F}$ as well, as compared to $(\text{BN})_3\text{OSO}_2\text{F}$ or even $(\text{BN})_2\text{OSO}_2\text{F}$ reported in Ref 18. Similar stoichiometry of $\text{C}_{6.6}\text{CN}$ has been seen for base-plane functionalized cyanographene and for its derivative graphene acid as well [79], despite that the parent fluorographene can have equal number of C and F atoms. While oxygen functionalized graphene can have a 1:1 carbon-to-oxygen ratio in graphene monoxide [88], the epoxy and hydroxyl groups on the surface of graphene can diffuse, agglomerate and react with each other leaving the surface of graphene as O_2 or H_2O molecules at temperatures over 70 °C [89]. Such a decomposition of graphene oxide is even faster in the presence of certain salts, such as potassium salts [56]. No such fast thermal decomposition is known for oxidized or hydroxyl functionalized h-BN. In fact, oxy-

gen functionalized h-BN is known to be stable over 800 °C [65].

The hopping of radicals between nearby carbon atoms on the surface of graphene is much less hindered energetically than in h-BN and leads to recombination of radicals between neighboring sites and ultimately to the detachment of these recombined radicals from graphene or even oxidation of carbon atoms. Fluorographene is the only known functionalized graphene that preserves a high degree of functionalization in a broad thermal window, up to 400 °C, albeit some decomposition starts on it above 100 °C [90]. In the base-plane functionalized h-BN, radicals are bound to boron atoms and the nitrogen atoms form barriers between nearest neighbor borons for the hopping of radicals hindering recombination reactions. For this reason, h-BN appears more suitable for dense, thermally stable surface functionalizations than graphite.

Edge vs basal plane functionalization

Both edge and basal plane functionalizations of 2D materials may be used as electroactive species in energy storage applications. However, the basal plane normally provides much larger number of functionalization sites than the edges, therefore the utilization of the basal plane functionalization is more advantageous for high capacity charge storage. The basal plane functionalization can also play the role of solvation shell for intercalating cations, i.e. it can be used as a solid electrolyte. This is much less the case for edge functionalizations, unless too many edges and lattice defects are introduced. However, too many lattice defects may reduce mechanical and structural stability. Therefore, basal plane functionalization appears inevitable for an efficient energy storage device based on 2D materials.

Graphene oxide (GO) normally contains both edge and basal plane functionalization. Oxo ($=\text{O}$) groups functionalize the edges through double bonds to single C atoms while epoxy ($-\text{O}-$) groups functionalize the basal plane through two single bonds to two nearest neighbor carbon atoms. In order to utilize graphene oxide as cathode electroactive species, one has to remove the epoxy groups by gentle heating, because they would irreversibly react with Li or Na and form Li_2O or Na_2O , as opposed to oxo groups which can be reduced and oxidized reversibly, at least when the temperature is not too high [36–38], albeit, as noted above the selection of suitable electrolytes is also critical for the cycling stability of the oxo groups and the conversion of the oxo groups to $-\text{OBF}_3^-$ groups appears to be one way to achieve this stability.

COMPARISON OF ELECTRONIC AND GEOMETRIC STRUCTURES OF $\cdot\text{OSO}_2\text{F}$, $\cdot\text{OBF}_3$ AND $\cdot\text{OBCl}_3$ FUNCTIONALIZED h-BN

The robust synthesis and thorough characterization of $\cdot\text{OSO}_2\text{F}$ functionalized h-BN, $(\text{BN})_2\text{OSO}_2\text{F}$ forty years ago [17] and its instability toward reductive species as well as its great electronic conductivity [18] and the great ionic conductivity of functionalized boron nitrides in general as reviewed above, motivated our re-design of $(\text{BN})_2\text{OSO}_2\text{F}$ in Ref. 16 with the goal of achieving a functionalization that preserves the excellent ionic and electronic conductivity while also providing structural stability against reductive species. While in Ref. 16 the electronic structures of oxygen, fluorene and $\cdot\text{OBF}_3$ functionalized h-BN were compared, here we provide the first ever report on the band structure of $(\text{BN})_2\text{OSO}_2\text{F}$ (synthesized and characterized forty years ago) as well as that of $\cdot\text{OBCl}_3$ functionalized h-BN and compare them to $\cdot\text{OBF}_3$ functionalized h-BN, along with the band structures of the related Li, Na and Mg reduced species. The effects of functionalization on the electronic and structural parameters of these species will also be discussed.

Computational methodology

Model systems for functionalized h-BN monolayers were built using a double stoichiometric formula unit of the respective compounds in order to allow for uniform functionalization on both the top and bottom surfaces of h-BN. Monolayers were separated from each other by a 30 Å distance that included about 22 Å vacuum layer while 3D periodic boundary conditions were applied. Similar surface slabs are often used to model surface chemistry and physics [91]. Supercells of the simulation cells are shown in Figs. 1 and 2.

Density Functional Theory (DFT) calculations were carried out using the Quantum Espresso program package [92, 93], following the methodology in our former works [15, 16, 77, 94]. A plane wave basis set with 50 Ry wave-function cut-off was used in conjunction with the PBEsol exchange-correlation functional [95, 96] and the related ultrasoft pseudopotentials as provided by the software package. A k-space grid of the size of $10 \times 10 \times 4$ (and twice this dense for h-BN) was employed to achieve mRy convergence of the electronic energy with respect to k-space saturation. This accuracy is satisfactory for the prediction of accurate cell voltages within the chosen exchange-correlation functional and surface model. As the radical functionalization of h-BN often results in open shell systems, spin polarized calculations were carried out. Since the model systems have the same translational symmetry as h-BN, only with larger unit cells, the representation of the electronic band structure employed the same high symmetry k-points. The coordinates of

the high symmetry points in the k-space are $\Gamma(0,0,0)$, $M(1/2,0,0)$ and $K(2/3,1/3,0)$.

The model systems were relaxed until residual forces on the atoms became smaller than 0.0001 Ry/bohr and residual pressure on the simulation cell was less than 3 kbar. Energies of cell reactions were calculated from electronic energy differences of products and starting materials, all in the crystal phase. Open cell voltages are computed as the negative of the cell reaction energies divided by the number of electrons transferred in the reaction. Capacity density values refer to the total charge of positive ions per mass of the discharged active material, expressed in units of mAh/g. Energy densities are obtained as the product of the open cell voltage and the corresponding capacity and expressed in Wh/kg units.

Löwdin charges were calculated by projecting the electron density from plane wave basis into atomic orbital basis. As the two representations span different Hilbert spaces, the projection does not preserve charge neutrality for the sum of charges in atomic orbital basis.

Validation of this methodology can be found in our earlier works [16, 94] and it includes experimental lattice parameters and enthalpies of formation of $\alpha\text{-Li}_3\text{BN}_2$, Li_3N , and h-BN. Experimental lattice parameters have been reproduced within 2.5% error while experimental enthalpies within 4% [94].

The PBEsol functional, as a GGA type functional, typically underestimates band gaps, for example by about 1 eV for h-BN [16, 97]. Despite this inaccuracy, it is in general capable to correctly estimate the relative size of band gaps in a group of similar compounds, such as functionalized h-BN species. Higher accuracy methods, such as the PBE0 [98, 99] or HSE [100] functionals are much more computationally expensive in a plane-wave basis therefore PBEsol remains a practical tool for investigating and selecting designer molecules for experimental testing.

Effect of functionalization on properties

Figs. 1 and 2 depict the structures of $(\text{BN})_2\text{OSO}_2\text{F}$, $\text{Li}[(\text{BN})_2\text{OBF}_3]$ and $(\text{BN})_2\text{OBCl}_3$ and its Li, Na or Mg reduced versions, with one Li, Na or Mg atom per formula unit. Images of $(\text{BN})_2\text{OBF}_3$ and its corresponding Na and Mg reduced versions can be found in our former work, Ref. [16]. The band structures of h-BN, $(\text{BN})_2\text{OSO}_2\text{F}$, $(\text{BN})_2\text{OBF}_3$, $(\text{BN})_2\text{OBCl}_3$ and the Li, Na and Mg reduced versions of the latter two ones are compared in Fig. 3. Table I lists electronic structure properties (band gaps, magnetizations, Löwdin charges) while Tables II and III the characteristic bond lengths and angles, respectively.

Figs. 3 a and b indicate the band structures of h-BN and $(\text{BN})_2\text{OSO}_2\text{F}$, respectively. The large calculated direct band gap of h-BN of 4.7 eV (experimental value 5.971 eV [101]) is reduced to zero upon functionalization

TABLE I: Calculated electronic structure properties of h-BN, $(\text{BN})_2\text{OSO}_2\text{F}$ and $\text{A}[(\text{BN})_2\text{OBX}_3]$ ($\text{A}=\text{Li,Na,Mg}$; $\text{X}=\text{F,Cl}$). Band gaps (E_g), total (tot) and absolute (abs) magnetizations (M) and Löwdin charges (Q) are shown. The range of Q values is given in e/100 units for B and -e/100 units for N. Band gaps of direct transitions are shown. $(\text{BN})_2\text{OBF}_3$ systems are antiferromagnetic, while $(\text{BN})_2\text{OBCl}_3$ and $(\text{BN})_2\text{OSO}_2\text{F}$ ones are ferromagnetic.

material	E_g	M (μ_B)		Q (e/100)	
	(eV)	tot	abs	B(+)	N(-)
h-BN	4.7	0.0	0.0	47	40
$(\text{BN})_2\text{OSO}_2\text{F}$	0.0	1.75	1.97	24-50	26-40
$(\text{BN})_2\text{OBF}_3$	0.8	0.13	3.28	29-53	18-25
$\text{Li}[(\text{BN})_2\text{OBF}_3]$	0.0	0.01	1.53	-4-51	13-48
$\text{Na}[(\text{BN})_2\text{OBF}_3]$	0.0	0.02	1.50	3-47	13-37
$\text{Mg}[(\text{BN})_2\text{OBF}_3]$	3.4	0.00	0.00	34-40	40-50
$(\text{BN})_2\text{OBCl}_3$	0.0	2.08	2.25	14-54	24-36
$\text{Li}[(\text{BN})_2\text{OBCl}_3]$	0.0	2.04	2.24	-4-51	12-49
$\text{Na}[(\text{BN})_2\text{OBCl}_3]$	0.0	2.02	2.22	5-47	12-34
$\text{Mg}[(\text{BN})_2\text{OBCl}_3]$	3.9	0.00	0.00	35-41	38-50

TABLE II: Calculated characteristic bond lengths in h-BN, $(\text{BN})_2\text{OSO}_2\text{F}$ and $\text{A}[(\text{BN})_2\text{OBX}_3]$ ($\text{A}=\text{Li,Na,Mg}$; $\text{X}=\text{F,Cl}$). The shorter B-O bond is always the one within the OBX_3 unit. There is an intramolecular fluorine transfer in $(\text{BN})_2\text{OBF}_3$ which has a structure of $(\text{BNF})(\text{BNOBF}_2)$ with the shorter B-F bond in the OBF_2 unit.

material	bond lengths (Å)		
	B-N	B-O	B-X
h-BN	1.45	—	—
$(\text{BN})_2\text{OSO}_2\text{F}$	1.50-1.60	—, 1.53	—
$(\text{BN})_2\text{OBF}_3$	1.58-1.61	1.37, 1.44	1.33, 1.41
$\text{Li}[(\text{BN})_2\text{OBF}_3]$	1.48-1.59	1.44, 1.46	1.42-1.45
$\text{Na}[(\text{BN})_2\text{OBF}_3]$	1.49-1.60	1.43, 1.45	1.42-1.45
$\text{Mg}[(\text{BN})_2\text{OBF}_3]$	1.49-1.59	1.40, 1.58	1.37, 1.48
$(\text{BN})_2\text{OBCl}_3$	1.47-1.58	1.34, 1.49	1.86-2.02
$\text{Li}[(\text{BN})_2\text{OBCl}_3]$	1.50-1.60	1.38, 1.48	1.85-1.98
$\text{Na}[(\text{BN})_2\text{OBCl}_3]$	1.49-1.59	1.36, 1.50	1.82-2.23
$\text{Mg}[(\text{BN})_2\text{OBCl}_3]$	1.49-1.62	1.42, 1.55	1.80-1.92

with the $\cdot\text{OSO}_2\text{F}$ radical in $(\text{BN})_2\text{OSO}_2\text{F}$. This is in qualitative agreement with the observed metallic conductivity of 1.5 S/cm in $(\text{BN})_2\text{OSO}_2\text{F}$ [18].

Calculations indicate ferromagnetic ground state in $(\text{BN})_2\text{OSO}_2\text{F}$ and in the $(\text{BN})_2\text{OBCl}_3$ systems, while antiferromagnetic ground state has been predicted for the $(\text{BN})_2\text{OBF}_3$ systems. Magnetic susceptibility measurements on $(\text{BN})_2\text{OSO}_2\text{F}$ found a paramagnetic behaviour [18], often seen in open shell systems with unpaired electrons. This is in agreement with the expectation that strongly oxidizing (electron withdrawing) radicals functionalizing the B sites create holes (electron deficiency) in the neighboring N atoms, decrease the electron density in

TABLE III: Calculated characteristic bond angles h-BN, $(\text{BN})_2\text{OSO}_2\text{F}$ and $\text{A}[(\text{BN})_2\text{OBX}_3]$ ($\text{A}=\text{Li,Na,Mg}$; $\text{X}=\text{F,Cl}$).

material	bond angles (deg)	
	N-B-O	B-O-(B,S)
h-BN	—	—
$(\text{BN})_2\text{OSO}_2\text{F}$	99-109	131-133
$(\text{BN})_2\text{OBF}_3$	99-110	143-146
$\text{Li}[(\text{BN})_2\text{OBF}_3]$	105-111	135
$\text{Na}[(\text{BN})_2\text{OBF}_3]$	101-109	136
$\text{Mg}[(\text{BN})_2\text{OBF}_3]$	100-110	138-140
$(\text{BN})_2\text{OBCl}_3$	105-111	134-149
$\text{Li}[(\text{BN})_2\text{OBCl}_3]$	101-110	135-136
$\text{Na}[(\text{BN})_2\text{OBCl}_3]$	102-110	132-133
$\text{Mg}[(\text{BN})_2\text{OBCl}_3]$	101-115	132-133

the lone pairs of the N atoms and in the B-N bonds [16]. This effect is also seen on the increased B-N bondlengths and strong deviation from planarity in the bond angles as shown in Table III. The atomic charges indicate similar tendency, the B and N atoms lose significant electron density upon functionalization. Upon reduction with Li, Na and Mg, the electron densities get partially restored, especially in the case of Mg reduction, as one Mg per formula unit donates two electrons.

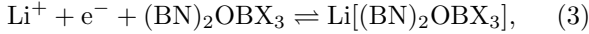
Note that the valence shell of the B atom is electron deficient by two electrons in h-BN [16], therefore each formula unit of $(\text{BN})_2\text{OSO}_2\text{F}$ could in principle take up three additional electrons, as one electron is provided by the functionalizing $\cdot\text{OSO}_2\text{F}$ radical. For simplicity of notation, X is used in the following, whenever a general reference to a halide, such as F or Cl, is made in these systems. $(\text{BN})_2\text{OBX}_3$ could in principle take up four electrons, as the B-O bond in the functionalizing $\cdot\text{OBX}_3$ radical can also take up an additional electron, as opposed to the S in the $\cdot\text{OSO}_2\text{F}$ which is saturated with valence +6.

In practice, only two electrons per formula unit of $(\text{BN})_2\text{OBX}_3$ can be taken up, each going formally into the two electron deficient B-O bonds in the B-O-B links between the h-BN substrate and the $\cdot\text{OBX}_3$ radical. The $(\text{BN})_2\text{OBX}_3$ system can also be viewed as an oxygen double radical sandwiched between a B center of the h-BN monolayer and the B of a neighboring BX_3 molecule, the latter being a strong Lewis acid. Once two electrons are taken up by the B-O-B links, the non-functionalized B atoms of $(\text{BN})_2\text{OBX}_3$ are not expected to absorb additional electrons in practice, as they are not strong enough Lewis acids, even though their valence shells are still incomplete by two electrons. More realistically, the electron deficient B-O- BX_3 links withdraw electrons from the nearby N atoms creating holes in them as soon as the functionalization is established and these N-holes will take up the electrons later provided by reductive Li, Na

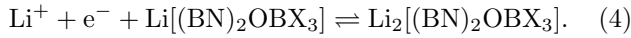
or Mg atoms or by any other suitable reductive agents. After the reduction of $(\text{BN})_2\text{OBX}_3$, the extra one or two electrons will largely be localized on the B-O bonds in the B-O-BX₃ links making these links once or twice negatively charged ions.

Some B-N bond-lengths in the $(\text{BN})_2\text{OBX}_3$ systems become as long as 1.62 Å, which is a substantial deviation from 1.45 Å seen in h-BN. However, such long B-N bonds are not unusual as the B-N bondlength in cubic BN is 1.57 Å (sphalerite type) or 1.55-1.58 Å (wurtzite type), 1.58 Å in ammonia borane ($\text{H}_3\text{N} \rightarrow \text{BH}_3$) and 1.66 Å in $\text{H}_3\text{N} \rightarrow \text{BF}_3$.

One possible application of the $(\text{BN})_2\text{OBX}_3$ systems is as cathode active species in electrochemical energy storage devices, such as batteries and super/pseudo-capacitors. In such applications, the reduction of the $(\text{BN})_2\text{OBX}_3$ species happens during discharge, for example as



and



In the present work, only one Li, Na or Mg atom is used to reduce the $(\text{BN})_2\text{OBX}_3$ materials per formula unit, however, in principle up to two Li or Na atoms or one Mg atom per formula unit can be absorbed to provide the two electrons that the above mentioned B-O-B links and the related N-holes can absorb. The reason for investigating only one reductive atom per formula unit here is that the first reductive atom can be placed within the monolayer between the functional groups, while the second atom would be placed between the monolayers and would require additional complexity of modeling that we will consider in a separate study. Nonetheless, it is worth mentioning that the absorption of a second electron per formula unit is expected to near double the capacity and energy density of the Li and Na based discharge processes. For Mg, the two electron absorption process is discussed here as the Mg^{2+} ion fits into the monolayer. The calculated open circuit voltages, gravimetric capacities and energy densities of the corresponding cell reactions are listed in Table IV.

The most energetic cell reaction happens between a Li anode and $\cdot\text{OBF}_3$ functionalized h-BN at a voltage of 5.6 V with a capacity of 191 mAh/g and energy density of 1067 Wh/kg. The voltage for this cathode material decreases to 5.1 V for Na anode and so does the capacity (171 mAh/g) and the energy density (874 Wh/kg) as well. With Mg anode, two electrons are absorbed, thus albeit the voltage decreases to 3.6 V, the capacity becomes 340 mAh/g and the energy density 1222 Wh/kg. Exchanging the F in the cathode to Cl still produces very energetic cell reactions with voltages of 3.69, 3.44 and 2.78 V while capacities are 141, 130 and 259 mAh/g and

TABLE IV: Calculated electrochemical properties of $(\text{BN})_2\text{OBX}_3$ (X=F,Cl) with Li, Na and Mg anodes. Open circuit voltage (OCV), gravimetric capacity (GC) and energy density (GED) values are shown. Discharged states investigated here contain one anode atom per formula unit, which is half of the theoretical maximum capacity of $(\text{BN})_2\text{OBX}_3$ for the Li and Na systems and full capacity for Mg.

	OCV	GC	GED
discharged state	(V)	(mAh/g)	(Wh/kg)
Li[(BN) ₂ OBF ₃]	5.60	191	1067
Na[(BN) ₂ OBF ₃]	5.10	171	874
Mg[(BN) ₂ OBF ₃]	3.60	340	1222
Li[(BN) ₂ OBCl ₃]	3.69	141	521
Na[(BN) ₂ OBCl ₃]	3.44	130	448
Mg[(BN) ₂ OBCl ₃]	2.78	259	719

energy densities 521, 448 and 719 Wh/kg, for Li, Na and Mg anodes (only one anode atom absorbed per formula unit), respectively.

The band gaps of the reduced systems are zero, as long as there is a sufficient concentration of N-holes in the system, i.e. until significantly less than two electrons per formula unit are absorbed. In the calculated discharged systems, the Li and Na discharged species still have zero band gap, while the Mg ones have a 3.4-3.9 eV band gap. The size of the band gap is informative about the expected electronic conductivity, albeit the latter also depends on the mobility of the charge carriers. Since the charge carriers are the N-holes in these systems, the electronic conductivity is likely to be similar to the baseline material $(\text{BN})_2\text{OSO}_2\text{F}$ and be in the order of 1.5 S/cm at room temperature [18]. As mentioned above, this electronic conductivity is in the same order with practical graphene (having lattice defects) and with carbon black conductive additives used in batteries.

The proton conductivity of functionalized h-BN is in the order of 0.1 S/cm at room temperature [102] and similarly great Li ion conductivities can be expected in the $\text{A}_n[(\text{BN})_2\text{OBX}_3]$ materials proposed here, where A is an alkali atom (Li, Na, etc; $0 \leq n \leq 2$) or alkaline earth (Mg, etc; $0 \leq n \leq 1$). This property will be discussed below in a separate section.

The combined features of the $\text{A}_n[(\text{BN})_2\text{OBX}_3]$ compounds allow for many valuable functions by a single material, such as electroactive species, solid ion conductors and potentially even as electroconductive material, at the same time. Reduction of the number of different phases in a (solid state) battery can be very helpful, for example for reducing interfacial impedance [87]. It is expected that $\text{A}_n[(\text{BN})_2\text{OBX}_3]$ are also stable at elevated temperatures and safe as only solid decomposition products are expected from them upon high temperature heating. These features will be discussed in forthcoming sections.

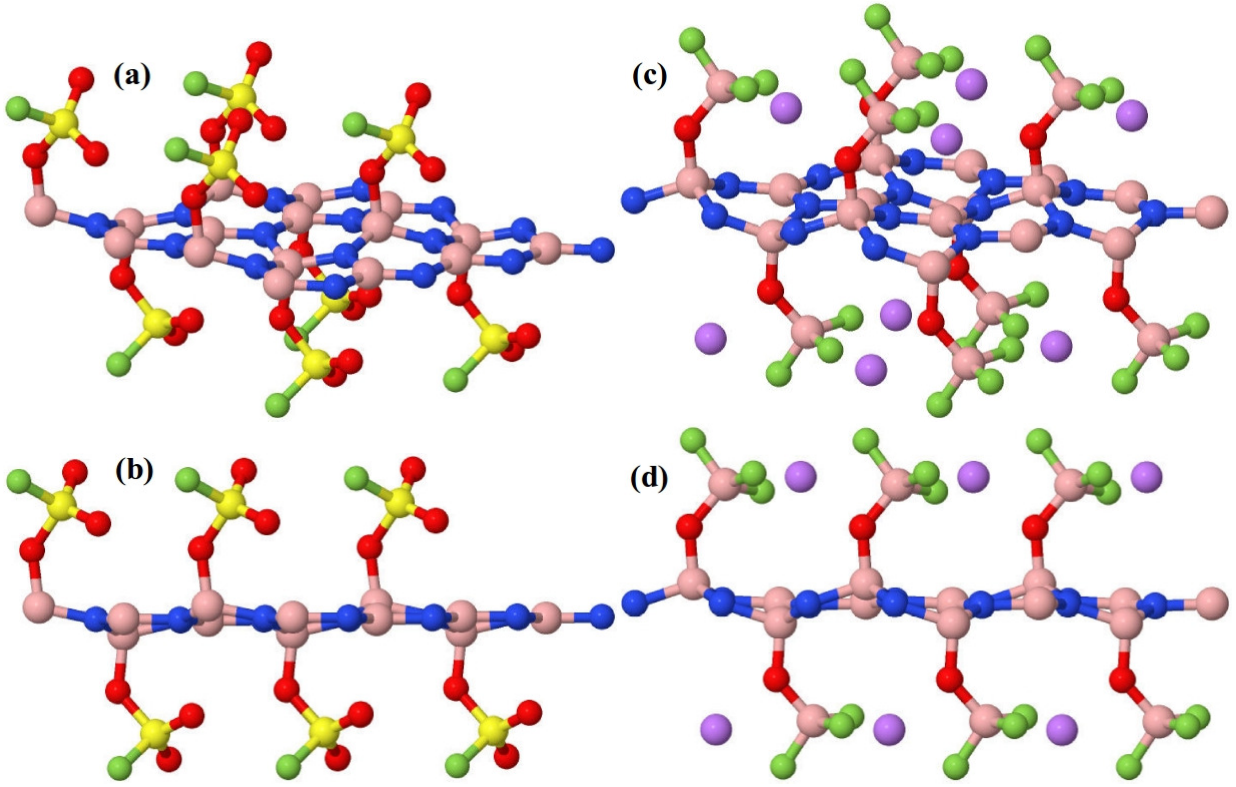
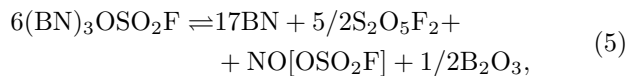


FIG. 1: Perspective and side views of 2x2 supercells of monolayers of $(\text{BN})_2\text{OSO}_2\text{F}$ (panels a and b) and $\text{Li}[(\text{BN})_2\text{OBF}_3]$ (panels c and d). They represent maximum density space filling functionalizations of the surface of a h-BN monolayer with the $\cdot\text{OSO}_2\text{F}$ radical and with the $\cdot\text{OBF}_3^-$ radical anion, with associated Li^+ for the latter, respectively. Color code: N – blue, B – bronze, O – red, S – yellow, F – green, Li – magenta. Structures represent optimum energy geometries of the respective surface slabs.

STABILITY OF FUNCTIONALIZED h-BN-S

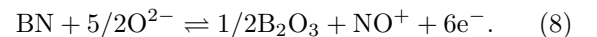
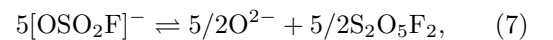
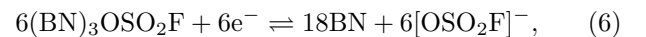
Stability of $\cdot\text{OSO}_2\text{F}$ functionalized h-BN

As described in Ref 18, $\cdot\text{OSO}_2\text{F}$ functionalized h-BN was stable over several months, unless it came in contact with base metals, in which case it quickly decomposed. Decomposition also happened when liquid HF, dried over K_2NiF_6 was distilled over samples of $\cdot\text{OSO}_2\text{F}$ functionalized h-BN. No decomposition happened with HF gas, indicating that traces of K_2NiF_6 , a transition metal salt, might be responsible for the decomposition of the h-BN derivative. Also, quantum chemical calculations in the present work indicate the detachment of $[\text{OSO}_2\text{F}]^-$ ions from h-BN, when $(\text{BN})_2\text{OSO}_2\text{F}$ is lithiated. The decomposition of a sample with $(\text{BN})_3\text{OSO}_2\text{F}$ stoichiometry was precisely measured [18] to happen according to



where $\text{S}_2\text{O}_5\text{F}_2$ has the structure of $\text{FSO}_2\text{-O-SO}_2\text{F}$ with a single oxygen atom between the fluorosulfonyl groups and $\text{NO}[\text{OSO}_2\text{F}]$ consists of a NO^+ (nitrosonium) cation and

a non-radical $[\text{OSO}_2\text{F}]^-$ anion formed from the charge neutral radical $\cdot\text{OSO}_2\text{F}$ after the absorption of an electron. The precise mechanism of this decomposition is unknown. The present author speculates, that it is catalytic amounts of dissolved transition metals that induce the detachment of $\cdot\text{OSO}_2\text{F}$ radicals from h-BN in the reduced form of $[\text{OSO}_2\text{F}]^-$ anions by transferring six electrons to these radicals, and on turn the transition metals recover these six electrons from the oxidation of a nitride ion of h-BN from oxidation number -3 to +3 resulting in the formation of a nitrosonium ion. Since the process of Eq 5 also involves the detachment of oxide ions from the $[\text{OSO}_2\text{F}]^-$ ions before $\text{S}_2\text{O}_5\text{F}_2$ forms, the process may also include the temporary valence change of the sulfur atoms. This speculated process may formally be partitioned into the following equations without claiming that they would describe the precise mechanism:



Since one of the reaction products of Eq 5, namely $\text{S}_2\text{O}_5\text{F}_2$, is volatile and is removed from the system, the equilibrium is shifted toward the complete decomposition

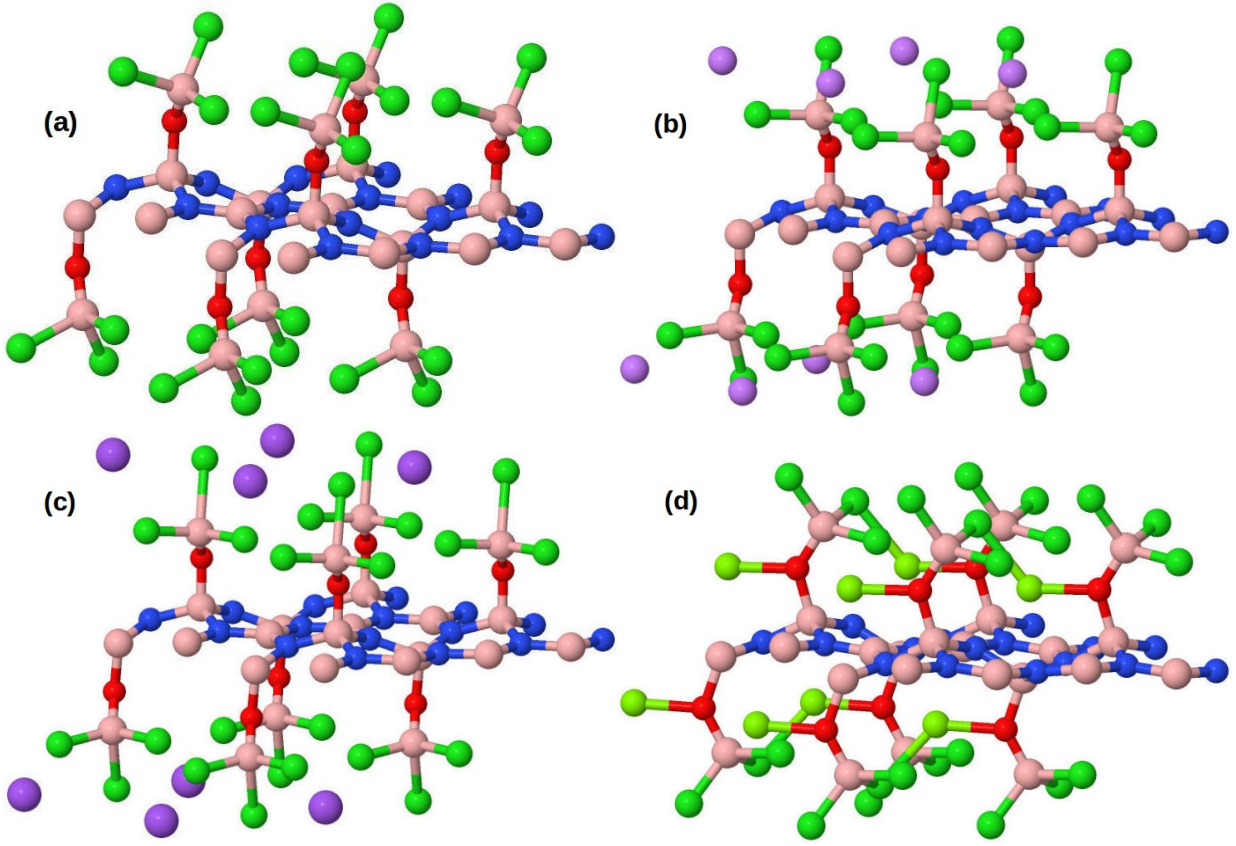


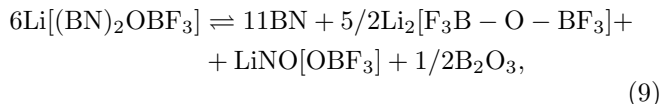
FIG. 2: Perspective views of 2x2 supercells of monolayers of $(\text{BN})_2\text{OBCl}_3$ (panel a) and its Li, Na and Mg reduced versions with one reducing atom per formula unit: $\text{Li}[(\text{BN})_2\text{OBCl}_3]$, $\text{Na}[(\text{BN})_2\text{OBCl}_3]$ and $\text{Mg}[(\text{BN})_2\text{OBCl}_3]$ (panels b through d, respectively). They represent maximum density space filling functionalizations of the surface of a h-BN monolayer with the given species. Color code: N – blue, B – bronze, O – red, Cl – green, Li – magenta, Na – purple, Mg light green. Structures represent optimum energy geometries of the respective surface slabs. Related structures with F instead of Cl in the OBCl_3 units have been depicted in our former work [16].

of $(\text{BN})_3\text{OSO}_2\text{F}$. Without a volatile product, the decomposition is expected to be slow if happening at all.

Stability of $\cdot\text{OBF}_3^-$ functionalized h-BN

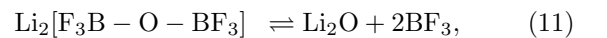
In the discharged state

Assuming that the decomposition of $\text{Li}[(\text{BN})_2\text{OBF}_3]$ would happen similarly to that of Eq 5, the analogous reaction would follow as:



where $[\text{F}_3\text{B}-\text{O}-\text{BF}_3]^{2-}$ is a Lewis adduct of an oxide ion with two BF_3 molecules and is an anionic ether, similar to the charge neutral ether $\text{FSO}_2-\text{O}-\text{SO}_2\text{F}$ in Eq 5. $\text{LiNO}[\text{OBF}_3]$ is a salt of the $[\text{OBF}_3]^{2-}$ anion with one NO^+ and one Li^+ cation. Both anions are non-radical ones and are also analogous to the well known BF_4^- anion with one F^- exchanged to an O^{2-} . Also note that

closely related nitrosonium tetrafluoroborate, $\text{NO}[\text{BF}_4]$ is a well known compound. All products of reaction Eq 9 – beside h-BN – are salts and are non-volatile. Therefore, it is expected that the decomposition of $\text{Li}[(\text{BN})_2\text{OBF}_3]$ would be much slower than that of $(\text{BN})_3\text{OSO}_2\text{F}$. Also the lack of a second valence changing atom – besides nitrogen – may hinder the decomposition: the structural equivalent of sulfur of $\cdot\text{OSO}_2\text{F}$ would be boron of $\cdot\text{OBF}_3^-$, which is not expected to change its valence in the given circumstances. Electrochemical extraction of the Li^+ ions (charging of the battery) may potentially even reverse this decomposition and produce the charged state of the system. At elevated temperatures the following additional decompositions may happen:



producing the only gaseous decomposition product, BF_3 . However, for such a decomposition to happen, ionic Lewis adducts must break up which is expected to require high temperatures similar to the decomposition temperature

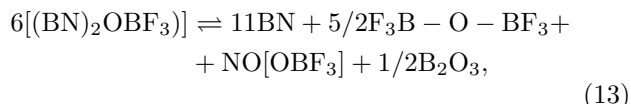
of LiBF₄ to LiF and BF₃ which happens between 162 and 277 °C with peak at 263 °C [103]. Even further, BF₃ can react with B₂O₃ to form solid boron-oxyfluoride, BOF:



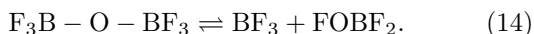
BOF may have several different structures, such as glass or six-membered rings and is stable even at very high temperatures [104, 105].

In the charged state

The fully charged state has the chemical formula (BN)₂OBF₃. In this state, the single radical $\cdot\text{OBF}_3^-$ anion is oxidized to a charge neutral double radical $:\text{OBF}_3$ which is the Lewis adduct of a double radical oxygen atom with BF₃. Then the charge neutral double radical $:\text{OBF}_3$ splits into two single radicals, according to theoretical predictions: one $\cdot\text{F}$ and one $\cdot\text{OBF}_2$ [16]. Each of these radicals functionalize separate nearby boron atoms as expressed by the formula (BNF)(BNOBF₂). Note that such a splitting of the $:\text{OBCl}_3$ radical has not been seen in the present calculations. Assuming a similar decomposition as in the above cases, the following is expected:



where F₃B-O-BF₃ is the Lewis adduct of an oxygen atom with two BF₃ molecules and NO[OBF₃] is the salt of a nitrosonium cation with a $\cdot\text{OBF}_3^-$ radical anion. F₃B-O-BF₃ may further decompose according to



Further, BF₃ gas may be bound through reaction with B₂O₃ to form solid BOF, as mentioned also above. Therefore, it is expected that most decomposition products will be solids even at elevated temperatures.

SYNTHETIC STRATEGIES

In the following subsections, synthetic strategies for the production of (BN)₂OBF₃ and its reduced states will be discussed. Analogous strategies can be applied for (BN)₂OBCl₃ and its reduced versions as well.

Charged state: (BN)₂OBF₃

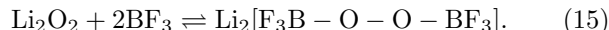
Perhaps the most efficient synthesis for the charged state of the proposed (BN)₂OBF₃ electroactive species is based on reacting h-BN with a mixture of ozone (O₃) and BF₃ in an inert medium, as proposed in our former work Ref 67. An ideal such medium for ozonation reactions is

liquid CO₂ in which high concentrations of ozone can be used safely [106, 107].

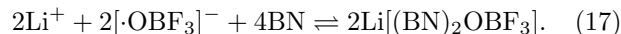
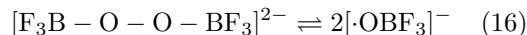
In a similar, but somewhat simpler setting proposed here, a mixture of concentrated H₂O₂ and a source of BF₃ [108], such as ether solution of BF₃ or BF₃ gas may be used to generate Lewis adducts H₂O₂·2BF₃ which spontaneously split to $\cdot\text{OHBF}_3$ radicals and these radicals covalently bind to the boron atoms of h-BN. The protons can be removed electrochemically to obtain (BN)₂OBF₃. Another equivalent of this latter process is to functionalize h-BN with $\cdot\text{OH}$ radicals first, then react the product with BF₃ [109] and extract the protons electrochemically.

Radical anion functionalization to obtain the discharged state: Li[(BN)₂OBF₃]

The robust and fast synthesis of (BN)₂OSO₂F carried out first in 1978 [17, 18], using liquid peroxide FSO₂-O-O-SO₂F as a source of $\cdot\text{OSO}_2\text{F}$ radicals, has inspired the present author to look for a similar peroxide based synthesis opportunity for the discharged state, Li[(BN)₂OBF₃], of the proposed cathode active material. By deleting the BN content of the formula Li[(BN)₂OBF₃], the remaining species would form Li[OBF₃] containing a Li⁺ cation and a $\cdot\text{OBF}_3^-$ radical anion. Such a radical anion can formally be derived from a salt Li₂[F₃B-O-O-BF₃] by splitting the peroxide bond in its [F₃B-O-O-BF₃]²⁻ anion. Since the BF₃ unit comes ultimately from BF₃ gas, this salt may be composed as the Lewis adduct of lithium peroxide Li₂O₂ with BF₃:



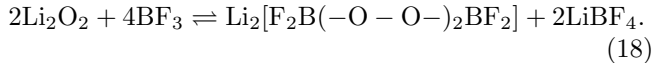
It is expected that melting Li₂[F₃B-O-O-BF₃] would lead to -O-O- bond splitting and the resulting radical anions would functionalize h-BN similarly to liquid FSO₂-O-O-SO₂F and the $\cdot\text{OSO}_2\text{F}$ radicals [109]:



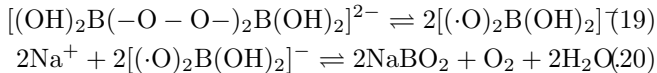
Lewis adducts, including adducts with BF₃, have been studied in past years as additives to liquid electrolytes that improve the performance of Li ion batteries [47–50]. In principle, the surface of cathode active species, such as the surface of LiCoO₂, can irreversibly bind BF₃ and other Lewis acids, as such binding has been known for Al₂O₃, SiO₂, TiO₂, ZrO₂, NiO, etc, resulting in M-OBF₂, M-OBF₃⁻ and (M)-O-(BF)₂-O-(M) surface functionalizations (M metal) [43–46]. The binding of Lewis acids to Lewis base surface sites may potentially be utilized in the construction of artificial solid-electrolyte interfaces.

Since the fluoride (halide) ions bound to boron have a great mobility in some solvents (such as in liquid boron trihalides) [110] the reaction of Li₂O₂ with BF₃ may have

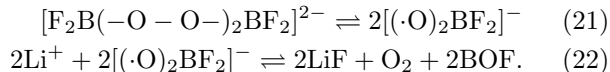
some alternative products as well, depending on the solvent and reaction circumstances. An alternative product would be a mixture of cyclic perborate $\text{Li}_2[\text{F}_2\text{B}(-\text{O}-\text{O}-)_2\text{BF}_2]$ and LiBF_4 :



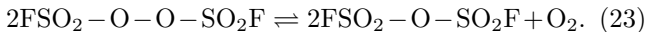
Such cyclic perborates are well known, for example sodium perborate $\text{Na}_2[(\text{OH})_2\text{B}(-\text{O}-\text{O}-)_2\text{B}(\text{OH})_2]$ is produced on the industrial scale for use as a bleaching agent. The thermal decomposition of sodium perborate has been studied and interpreted to go through the simultaneous splitting of both peroxide bonds to form radical anion species $[\text{O}_2\text{B}(\text{OH})_2]^-$ that is followed by the release of water and formation of sodium metaborate [42]:



Obviously, the analogous reaction with F instead of OH groups would not happen as it should release F_2 molecules instead of O_2 and H_2O , but F_2 is extremely reactive. Instead, the formation of BOF could be expected:



In light of the latter decomposition process, one must be careful to raise the temperature only up to the point of breaking the peroxide bonds (Eqns 16 and 21), but not to release O_2 , so that the $[(\cdot\text{O})_2\text{BF}_2]^-$ and $\cdot\text{OBF}_3^-$ radical anions can functionalize h-BN. This latter condition is however not surprising, it has been the same for the old, $\cdot\text{OSO}_2\text{F}$ functionalization of h-BN: would the temperature be too high, an explosive decomposition of the reagent $\text{FSO}_2-\text{O}-\text{O}-\text{SO}_2\text{F}$ could happen:



However, when carefully handled, as in Refs 17 and 18, even the distillation of $\text{FSO}_2-\text{O}-\text{O}-\text{SO}_2\text{F}$ could be carried out without explosive decomposition. Therefore, it is expected that the Lewis adducts of Li_2O_2 with BF_3 will also be stable in a temperature range above their melting points and can generate stable radical anions for the functionalization of h-BN. Both above mentioned radical anions $\cdot\text{OBF}_3^-$ and $[(\cdot\text{O})_2\text{BF}_2]^-$ are suitable to functionalize h-BN and both products can be used as cathode active species in batteries. Also note that $[(\cdot\text{O})_2\text{BF}_2]^-$ radical anions will occur in pair with BF_4^- as pointed out in Eq 18. This does not hinder the functionalization of h-BN, or the use of the product of the functionalization as cathode active species: BF_4^- ions would be part of the (solid) electrolyte surrounding the functionalized h-BN.

Radical anions from $\text{H}_2\text{O}.\text{BF}_3$ derivatives

An alternative source of $\cdot\text{OBF}_3^-$ radical anions may be based on the well known Lewis adduct of water with BF_3 , $\text{H}_2\text{O}.\text{BF}_3$, and its salts, such as $\text{LiOH}.\text{BF}_3$ and $\text{Li}_2\text{O}.\text{BF}_3$. Electrochemical extraction of one hydrogen or one alkali atom per formula unit results in salts (LiOBF_3) and Brønsted acids (HOBF_3) containing the desired radical anion. Therefore, a mixing of these derivatives of $\text{H}_2\text{O}.\text{BF}_3$ with h-BN and electrolysis of the mixture will likely result in $\cdot\text{OBF}_3^-$ -functionalized h-BN. While NaHOBF_3 has been synthesized by the reaction of NaHCO_3 and BF_3 in aqueous solution [111, 112], the analogous LiOBF_3 has not been synthesized yet [113]. Nothing is known of Li_2OBF_3 either. $\text{H}_2\text{O}.\text{BF}_3$ itself hydrolyzes in water to boric acid, HF and a number of other intermediates [114]. Therefore, it appears that routes to $\cdot\text{OBF}_3^-$ based on derivatives of $\text{H}_2\text{O}.\text{BF}_3$ are less certain and less efficient than those based on peroxide bond splitting, except perhaps the route based on NaHOBF_3 which can be synthesized in a very economic fashion.

Radical anions other than $\cdot\text{OBF}_3^-$

The functionalization of 2D materials with general radical anions other than $\cdot\text{OBF}_3^-$ is entirely possible. One such possibility is through splitting the N-N bond in Lewis adducts of hydrazine and BF_3 . Such adducts with $\text{H}_4\text{N}_2.\text{BF}_3$ or $\text{H}_4\text{N}_2.2\text{BF}_3$ composition are known, they form acidic solutions in water even before hydrolysis [115]. The splitting of the N-N bond of these compounds results in radical anions, such as $[\cdot\text{NHBf}_3]^-$ and protons. Functionalization of h-BN with these radical anions produces Brønsted acid functionalized h-BN. The N-protons can at least partially be exchanged to Li^+ or other cations electrochemically and be used as the discharged state of electroactive species.

OPTIMIZING THE EXTENT OF THE DISCHARGE

In principle, absorption of up to two electrons per formula unit of $(\text{BN})_2\text{OBX}_3$ is possible, therefore the general formula for the discharged state with Li anode and $(\text{BN})_2\text{OBF}_3$ cathode is $\text{Li}_n[(\text{BN})_2\text{OBF}_3]$ with $0 < n \leq 2$. For discharge $1 < n \leq 2$, however, the radical character of the functionalizing $\cdot\text{OBF}_3^-$ species will be lost when they pick up an additional electron and become $[\text{OBF}_3]^{2-}$. Once the radical character is lost, the anion may still be bound to the boron atom of h-BN if there is a sufficiently strong Lewis base (anion) and Lewis acid (B of h-BN) interaction between them. Unfortunately, the boron atom of a planar h-BN is a too weak Lewis acid as the planarity is strongly preferred due to the short B-N bonds.

However, the detachment of $[OBF_3]^{2-}$ anions is likely not irreversible, as charging of the battery re-creates the radical anions. Detachment of $[OBF_3]^{2-}$ is not expected from the edges of the h-BN layers as the B atoms there have much stronger Lewis acid character than in the middle of the basal plane. The electronic conductivity of the discharged state for $1 < n \leq 2$ will be much lower though than for $0 < n \leq 1$, because the concentration of N-holes decreases as $1 < n$ and $n \rightarrow 2$ and this leads to greater electronic resistance and less energy efficient recharge. A similar dependence of electronic conductivity on the concentration of hole states has been the conclusion of Ref 18 on the $-OSO_2F$ functionalized h-BN. Clearly, there is a trade-off between increased energy density and energy efficiency of charging.

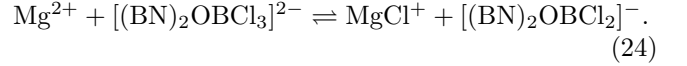
$A_n[(BN)_2OBX_3]$ AS A SOLID ELECTROLYTE

As high as 0.2 mS/cm room temperature Li-ion conductivity has been demonstrated in h-BN composite pastes containing h-BN, an absorbed ionic liquid electrolyte and a Li-salt [25]. The thermal stability of Li-ion batteries with this paste electrolyte has also been demonstrated up to 120 °C, which is well above 60 °C, the upper thermal limit of liquid electrolyte based batteries [25]. While Ref. 25 mentions the interaction of the electrolyte with h-BN, there was no indication of covalent functionalization of h-BN. Ion gel electrolytes containing amine functionalized h-BN show even higher Li-ion conductivity of 0.647 mS/cm at room temperature [116].

Similarly great proton-conductivity of h-BN-s functionalized with $\cdot OH$, $\cdot SO_3H$, $\cdot SO_3H$ and $\cdot NH_2$ radicals has been experimentally measured and found to be in the order of 0.1 S/cm when the functionalization was sufficiently dense [69–71]. This is a result of contiguous networks of hydrogen bridges between neighboring functional groups that allow for quick proton hopping. It suggests that some covalently functionalized h-BN-s may also be well suited for the conduction of other cations, such as Li^+ , Na^+ , Mg^{2+} and MgX^+ . Radical anion functionalization appears essential to fulfill this promise as it establishes a stable covalent binding of negatively charged functional groups to the surface of h-BN.

The $\cdot OBX_3$ functionalized 2D materials can particularly be advantageous for the transport of Mg^{2+} ions. In fact, Mg^{2+} ions often travel together with an attached halide ion [20]. This attached halide ion may come from the $\cdot OBX_3$ units, as the halide ions can quickly and reversibly separate from the boron centers, especially when the B center is negatively charged and three or four halides are attached to it [110]. An example of this process with Cl^- ions can be described by the following equation:

tion:



Therefore, the hopping of MgX^+ cations between $\cdot OBX_2$ sites is expected to be a fast way of transporting Mg^{2+} ions in the $\cdot OBX_3$ functionalized h-BN.

The recently discovered paddle wheel mechanism [117] also supports the use of the $\cdot OBX_3$ functional groups for achieving fast ion conduction in solids, as the rotation of these groups around the O-B bonds promotes the fast motion of cations, similarly to the Grotthuss mechanism of proton transfer that involves a hopping of protons between sites and rotations of the protonated sites.

The radical anions of the h-BN surface also provide a solvation shell for the cations. Even with dense functionalization, when every second B atom is functionalized with $\cdot OBF_3^-$, there is sufficient space between these anions for the quick hopping of cations between sites. Since the functionalized h-BN is intended to be used not only as an ionic conductor, but also as an electroactive species, the transport of positive ions must be coupled with the transport of equal number of electrons. N-holes generated by the electron withdrawing effect of the functionalizing anionic radicals are the enablers of efficient electronic transport [16]. A similar role of O-holes have been observed in $LiCoO_2$, albeit the transport of electrons is only partially based on O-holes and to a greater extent to valence changes of cobalt [118–121].

$A_n[(BN)_2OBX_3]$ AS AN ANODE COATING AND SEPARATOR

Graphite fluoride (CF_x) was recently proposed as a coating/packaging material for lithium metal anodes [122]. It provides well-wetting surfaces to (solid) electrolytes, sufficient ionic conductivity, inertness to air and moisture, and dendrite-free cycling over hundreds of cycles. It appears to provide some temperature resistance as well, considering that the synthesis of the coating was performed at 250 °C. Contrary to the expectation that all the fluorene of CF_x should convert to LiF when in contact with lithium, this conversion does not seem to complete, while some LiF layers form between Li metal and CF_x .

Other proposed alternatives to CF_x coating include $g-C_3N_4$, which forms a Li_3N and graphene layer over the Li metal anode [123] or a biomineralization based coating using $-O-CH_2CF_3$ functionalized egg-shell-membrane [124] that allows for stable cycling of a Li metal anode for 3000 cycles at 5 mA/cm² current density.

Also note that highly fluorinated electrolytes have been known for long to allow for dendrite-free plating of lithium. These electrolytes include fluorosulfonyl imides [125, 126] and Lewis adducts of BF_3 with organic imides

and carboxylates [127–129].

$A_n[(BN)_2OBX_3]$ is expected to provide a similar coating on the respective metal anodes, except that it would not repel water, however it could potentially provide a greater thermal stability and ionic conductivity. Also note that BF_3 is a fire extinguishing agent for magnesium and, if released by thermal decomposition of the coating, could potentially help to suppress anode fires. The main advantage of $A_n[(BN)_2OBX_3]$ coating as compared to CF_x is likely a greatly increased ionic conductivity since the Li, Na and Mg fluorides have poor ionic conductivities, for example for the small size of their anions [130]. Much larger anions in $A_n[(BN)_2OBX_3]$ and a lot of space between the functional groups on the h-BN monolayers is expected to promote an improved ionic conductivity.

Similarly to all-solid-state graphene oxide batteries, where graphene oxide plays both the role of the cathode active species and the separator [52], $A_n[(BN)_2OBX_3]$ is also expected to be able to function as the separator as well. In this case, the fully reduced and therefore electronically isolating but ionically conducting $A_n[(BN)_2OBX_3]$ material would form the separator between the metal anode and the cathode, where $n=2$ for Li and Na and $n=1$ for Mg in the fully reduced states. The fully reduced species would naturally form upon direct contact of $A_n[(BN)_2OBX_3]$ with the anode. If mechanical enforcement is needed, $A_n[(BN)_2OBX_3]$ can be used as a component of a polymer-composite for the separator and also in the cathode.

COST ANALYSIS

Table V lists the materials-only cost of the battery components and the cost of storing 1 kWh energy. The theoretical energy densities were taken from Table IV. It is assumed that $A_n[(BN)_2OBX_3]$ is made of h-BN, BF_3 , BCl_3 and Li, Na or Mg metal (for A) and these materials are available at the following actual prices of 35, 20, 10, 85, 3.0 and 2.3 USD/kg [131], respectively (cost of oxygen has been neglected). It appears, the proposed battery materials are sufficiently cost effective, especially compared to the current cost of batteries, 156 USD/kWh [132], albeit labor, equipment and related costs are not included here.

SUMMARY AND CONCLUSIONS

Motivated by a forty years old functionalized h-BN material, $(BN)_2OSO_2F$ [17, 18] and its good electronic conductivity and instability toward reducing agents as well as by the outstanding energy and power densities of graphene oxide cathodes [36–38] and the instability of graphene oxide at elevated temperatures [57], a new cath-

TABLE V: Estimated price of materials and stored energy.

material	components	
	USD/kg	USD/kWh
Li $[(BN)_2OBF_3]$	26	24
Na $[(BN)_2OBF_3]$	20	23
Mg $[(BN)_2OBF_3]$	20	16
Li $[(BN)_2OBCl_3]$	18	35
Na $[(BN)_2OBCl_3]$	14	32
Mg $[(BN)_2OBCl_3]$	14	20

ode material has been proposed and analyzed here following up our earlier work in Ref. [16]. The new cathode material is based on $(BN)_2OBX_3$ (X is halide, such as F or Cl) and it may be used with Li, Na or Mg anodes forming discharge products $A_n[(BN)_2OBX_3]$, where A is an alkali atom (Li, Na, etc; $0 \leq n \leq 2$) or alkaline earth (Mg, etc; $0 \leq n \leq 1$). The discharged state with one Li, Na or Mg per formula unit may be synthesized by the thermal splitting of the Lewis adduct of the respective peroxide, such as Li_2O_2 , with BX_3 , and the resulting $\cdot OBX_3^-$ radical anions functionalize the h-BN monolayers in the presence of their respective cations. The radical anion functionalization method can be extended to other 2D materials as well, to tune their properties, especially ionic and electronic conductivities. $A_n[(BN)_2OBX_3]$ is predicted to have much greater thermal stability than graphene oxide while providing similarly great energy and power densities. It is also predicted to have good electronic and excellent ionic conductivity and can potentially be used simultaneously as a cathode active species and a solid electrolyte. Additional applications may include coating for metallic Li, Na and Mg anodes, separators and polymer composites. The manufacturing of the proposed materials appears to be economic.

ACKNOWLEDGEMENTS

The author thanks Prof. Leon Shaw (IIT) for calling his attention to the similarity of electronic conductivity values of $(BN)_2OSO_2F$ (first synthesized 1978 [17, 18]) and that of practical graphene and conductive carbon additives used in batteries. The use of computational resources at NERSC (U.S. DOE DE-AC02-05CH11231), a U.S. Department of Energy Office of Science User Facility, is gratefully acknowledged.

-
- [1] M Stanley Whittingham. Electrical energy storage and intercalation chemistry. *Science*, 192(4244):1126–1127, 1976.
 - [2] NA Godshall, ID Raistrick, and RA Huggins. Thermodynamic investigations of ternary lithium-transition

- metal-oxygen cathode materials. *Materials Research Bulletin*, 15(5):561–570, 1980.
- [3] K. Mizushima, P.C. Jones, P.J. Wiseman, and J.B. Goodenough. Li_xCoO_2 ($0 < x < 1$): A new cathode material for batteries of high energy density. *Materials Res. Bull.*, 15:783, 1980.
 - [4] Michael M. Thackeray, Christopher S. Johnson, Khalil Amine, and Jaekook Kim. Lithium metal oxide electrodes for lithium cells and batteries, 2001. US Patent 6677082B2.
 - [5] Michael M. Thackeray, Christopher S. Johnson, Khalil Amine, and Jaekook Kim. Lithium metal oxide electrodes for lithium cells and batteries, 2001. US Patent 6680143B2.
 - [6] Zhonghua Lu and Jeffrey R. Dahn. Cathode compositions for lithium-ion batteries, 2001. US Patent 6964828B2.
 - [7] CH Chen, J Liu, ME Stoll, G Henriksen, DR Vissers, and K Amine. Aluminum-doped lithium nickel cobalt oxide electrodes for high-power lithium-ion batteries. *Journal of power Sources*, 128(2):278–285, 2004.
 - [8] Akira Yoshino, Kenichi Sanekikawa, and Takayuki Nakajima. Secondary battery, 1986. US Patent 4668595A.
 - [9] R. Yazami and Ph. Touzain. A reversible graphite-lithium negative electrode for electrochemical generators. *J. Power Sources*, 9:365, 1983.
 - [10] Lin Chen and Leon L Shaw. Recent advances in lithium-sulfur batteries. *Journal of Power Sources*, 267:770–783, 2014.
 - [11] Quan Pang, Chun Yuen Kwok, Dipan Kundu, Xiao Liang, and Linda F Nazar. Lightweight metallic mgb2 mediates polysulfide redox and promises high-energy-density lithium-sulfur batteries. *Joule*, 3(1):136–148, 2019.
 - [12] Maziar Ashuri, Qianran He, and Leon L Shaw. Silicon as a potential anode material for li-ion batteries: where size, geometry and structure matter. *Nanoscale*, 8(1):74–103, 2016.
 - [13] K. Nemeth. Functionalized boron nitride materials as electroactive species in electrochemical energy storage devices, 2015. WO/2015/006161.
 - [14] Karoly Nemeth. Functionalized boron nitride materials as electroactive species in electrochemical energy storage devices, 2020. US Patent 10,693,137.
 - [15] Károly Németh. Materials design by quantum-chemical and other theoretical/computational means: Applications to energy storage and photoemissive materials. *International Journal of Quantum Chemistry*, 114(16):1031–1035, 2014.
 - [16] Károly Németh. Simultaneous oxygen and boron trifluoride functionalization of hexagonal boron nitride: a designer cathode material for energy storage. *Theoretical Chemistry Accounts*, 137(11):157, 2018.
 - [17] Neil Bartlett, RN Biagioni, BW McQuillan, AS Robertson, and AC Thompson. Novel salts of graphite and a boron nitride salt. *Journal of the Chemical Society, Chemical Communications*, 5:200–201, 1978.
 - [18] Ciping Shen, Steven G Mayorga, Richard Biagioni, Charles Piskoti, Masahiro Ishigami, Alexander Zettl, and Neil Bartlett. Intercalation of hexagonal boron nitride by strong oxidizers and evidence for the metallic nature of the products. *Journal of Solid State Chemistry*, 147(1):74–81, 1999.
 - [19] Robert Ellis Doe, Craig Michael Downie, Christopher Fischer, George Hamilton Lane, Dane Morgan, Josh Nevin, Gerbrand Ceder, Kristin Aslaug Persson, and David Eaglesham. Layered materials with improved magnesium intercalation for rechargeable magnesium ion cells, 2013. US Patent 9401528B2.
 - [20] Yan Yao and Hyun Deog Yoo. Method of activating two-dimensional materials for multivalent/polyatomic-ion intercalation battery electrodes, 2018. US Patent appl. US20180183038A1.
 - [21] Hyun Deog Yoo, Yanliang Liang, Hui Dong, Junhao Lin, Hua Wang, Yisheng Liu, Lu Ma, Tianpin Wu, Yifei Li, Qiang Ru, et al. Fast kinetics of magnesium monochloride cations in interlayer-expanded titanium disulfide for magnesium rechargeable batteries. *Nature communications*, 8(1):339, 2017.
 - [22] Michael A. Zimmerman, Randy Leising, Alexei B. Gavrilo, Keith Smith, and Andy Teoli. High capacity polymer cathode and high energy density rechargeable cell comprising the cathode, 2015. US Patent appl. 0280218A1.
 - [23] Michael A. Zimmerman. Solid electrolyte high energy battery, 2017. US Patent 9819053B1.
 - [24] O. Ergen and A.K. Zettl. High temperature li-ion battery cells utilizing boron nitride aerogels and boron nitride nanotubes, 2018. US Patent appl. 0159180.
 - [25] Marco-Tulio F Rodrigues, Kaushik Kalaga, Hemtej Gulapalli, Ganguli Babu, Arava Leela Mohana Reddy, and Pulickel M Ajayan. Hexagonal boron nitride-based electrolyte composite for li-ion battery operation from room temperature to 150 c. *Advanced Energy Materials*, 6(12):1600218, 2016.
 - [26] Qian Cheng, Aijun Li, Na Li, Shuang Li, Amirali Zangibadi, Wenlong Huang, Alex Ceng Li, Tianwei Jin, Qingquan Song, Weiheng Xu, et al. Stabilizing solid electrolyte-anode interface in li-metal batteries by boron nitride-based nanocomposite coating. *Joule*, 3(6):1510–1522, 2019.
 - [27] Bao Shen, Tian-Wen Zhang, Yi-Chen Yin, Zheng-Xin Zhu, Lei-Lei Lu, Cheng Ma, Fei Zhou, and Hong-Bin Yao. Chemically exfoliated boron nitride nanosheets form robust interfacial layers for stable solid-state li metal batteries. *Chemical Communications*, 55(53):7703–7706, 2019.
 - [28] Md Mokhlesur Rahman, Srikanth Mateti, Qiran Cai, Irin Sultana, Ye Fan, Xinwei Wang, Chunping Hou, and Ying Chen. High temperature and high rate lithium-ion batteries with boron nitride nanotubes coated polypropylene separators. *Energy Storage Materials*, 19:352–359, 2019.
 - [29] L Staudenmaier. Verfahren zur darstellung der graphitsäure. *Berichte der deutschen chemischen Gesellschaft*, 31(2):1481–1487, 1898.
 - [30] Benjamin Collins Brodie. Xiii. on the atomic weight of graphite. *Philosophical Transactions of the Royal Society of London*, 149:249–259, 1859.
 - [31] William S Hummers Jr and Richard E Offeman. Preparation of graphitic oxide. *Journal of the american chemical society*, 80(6):1339–1339, 1958.
 - [32] Tamás Szabó, Ottó Berkési, Péter Forgó, Katalin Josepovits, Yiannis Sanakis, Dimitris Petridis, and Imre Dékány. Evolution of surface functional groups in a series of progressively oxidized graphite oxides. *Chemistry of materials*, 18(11):2740–2749, 2006.
 - [33] A.M. Dimiev and S. Eigler. *Graphene Oxide: Funda-*

- mentals and Applications*. Wiley, 2016.
- [34] Daniel R Dreyer, Sungjin Park, Christopher W Bielawski, and Rodney S Ruoff. The chemistry of graphene oxide. *Chemical society reviews*, 39(1):228–240, 2010.
- [35] Nina I Kovtyukhova, Yuanxi Wang, Ruitao Lv, Mauricio Terrones, Vincent H Crespi, and Thomas E Mallouk. Reversible intercalation of hexagonal boron nitride with brønsted acids. *Journal of the American Chemical Society*, 135(22):8372–8381, 2013.
- [36] Bor Z Jang, Chenguang Liu, David Neff, Zhenning Yu, Ming C Wang, Wei Xiong, and Aruna Zhamu. Graphene surface-enabled lithium ion-exchanging cells: next-generation high-power energy storage devices. *Nano Letters*, 11(9):3785–3791, 2011.
- [37] C. Liu, A. Zhamu, D. Neff, and B.Z. Jang. Lithium super-battery with a functionalized nano graphene cathode, 2014. US Patent 8795899B2.
- [38] Haegyeom Kim, Young-Uk Park, Kyu-Young Park, Hee-Dae Lim, Jihyun Hong, and Kisuk Kang. Novel transition-metal-free cathode for high energy and power sodium rechargeable batteries. *Nano Energy*, 4:97–104, 2014.
- [39] Haegyeom Kim, Kyu-Young Park, Jihyun Hong, and Kisuk Kang. All-graphene-battery: bridging the gap between supercapacitors and lithium ion batteries. *Scientific reports*, 4:5278, 2014.
- [40] G. I. Petrenko. Derivatives of perboric acid. *J. Russ. Phys. Chem. Soc.*, 34:37–42, 1902. <https://books.google.com/books?id=7fU4AAAAMAAJ>, page 317.
- [41] Khokan Samanta, Surajit Some, Youngmin Kim, Yeohung Yoon, Misook Min, Sae Mi Lee, Younghun Park, and Hyoyoung Lee. Highly hydrophilic and insulating fluorinated reduced graphene oxide. *Chemical Communications*, 49(79):8991–8993, 2013.
- [42] Nobuyoshi Koga, Nao Kamenoi, Yoji Tsuboi, Takayuki Fujiwara, Masayoshi Nakano, Kazuyuki Nishikawa, and Akiko Iwasaki Murata. Multistep thermal decomposition of granular sodium perborate tetrahydrate: A kinetic approach to complex reactions in solid-gas systems. *Physical Chemistry Chemical Physics*, 20(18):12557–12573, 2018.
- [43] Charles Joseph Plank. Catalytic conversion of hydrocarbons, 1947. US Patent US2428741A.
- [44] Kee H Rhee and Michael R Basila. Chemisorption of bf₃ on catalytic oxide surfaces: Infrared spectroscopic studies. *Journal of Catalysis*, 10(3):243–251, 1968.
- [45] BA Morrow, IA Cody, and Lydia SM Lee. Infrared studies of reactions on oxide surfaces. 7. mechanism of the adsorption of water and ammonia on dehydroxylated silica. *The Journal of Physical Chemistry*, 80(25):2761–2767, 1976.
- [46] BFMB Sadeghi, BF Mirjalili, and MM Hashemi. Bf₃ sio₂: An efficient heterogeneous alternative for regio-chemo and stereoselective claisen-schmidt condensation. *Journal of the Iranian Chemical Society*, 5(4):694–698, 2008.
- [47] Mengyun Nie, L Madec, J Xia, DS Hall, and JR Dahn. Some lewis acid-base adducts involving boron trifluoride as electrolyte additives for lithium ion cells. *Journal of Power Sources*, 328:433–442, 2016.
- [48] Ang Xiao, William M. Lamanna, Jeffrey R. Dahn, Mengyun Nie, Kiah A. Smith, and Vincent J. Chevrier. Electrochemical cells that include lewis acid: lewis base complex electrolyte additives, 2016. Patent appl. WO/2016/126534A1.
- [49] Masaki Matsui. Asymmetric type BF₃ complex, 2014. US Patent 8765294B2.
- [50] Yu Wang, Meijie Zhang, Ulrich Von Sacken, and Brian Michael Way. Additives for improving cycle life of non-aqueous rechargeable lithium batteries, 2000. US Patent US/6045948A.
- [51] Emily V Carino, Charles E Diesendruck, Jeffrey S Moore, Larry A Curtiss, Rajeev S Assary, and Fikile R Brushett. Bf₃-promoted electrochemical properties of quinoxaline in propylene carbonate. *RSC Advances*, 5(24):18822–18831, 2015.
- [52] Minghui Ye, Jian Gao, Yukun Xiao, Tong Xu, Yang Zhao, and Liangti Qu. Metal/graphene oxide batteries. *Carbon*, 125:299–307, 2017.
- [53] Gundu Venkateswarlu, Devarapaga Madhu, and Jeti Vatsala Rani. An effective performance of f-doped hexagonal boron nitride nanosheets as cathode material in magnesium battery. *Materials Chemistry and Physics*, 226:356–361, 2019.
- [54] Nobuatsu Watanabe and Masataro Fukuda. Primary cell for electric batteries, 1970. US Patent 3536532A.
- [55] Shiro Entani, Konstantin V Larionov, Zakhar I Popov, Masaru Takizawa, Masaki Mizuguchi, Hideo Watanabe, Songtian Li, Hiroshi Naramoto, Pavel B Sorokin, and Seiji Sakai. Non-chemical fluorination of hexagonal boron nitride by high-energy ion irradiation. *Nanotechnology*, 31(12):125705, 2020.
- [56] Franklin Kim, Jiayan Luo, Rodolfo Cruz-Silva, Laura J Cote, Kwonnam Sohn, and Jiaxing Huang. Self-propagating domino-like reactions in oxidized graphite. *Advanced Functional Materials*, 20(17):2867–2873, 2010.
- [57] Deepti Krishnan, Franklin Kim, Jiayan Luo, Rodolfo Cruz-Silva, Laura J Cote, Hee Dong Jang, and Jiaxing Huang. Energetic graphene oxide: challenges and opportunities. *Nano today*, 7(2):137–152, 2012.
- [58] Sean E Lowe and Yu Lin Zhong. Challenges of industrial-scale graphene oxide production. *Graphene Oxide: Fundamentals and Applications; Dimiev AM, Eigler S., Eds*, pages 410–431, 2017.
- [59] Li Lin, Hailin Peng, and Zhongfan Liu. Synthesis challenges for graphene industry. *Nature materials*, 18(6):520–524, 2019.
- [60] T Ikuno, T Sainsbury, D Okawa, JMJ Fréchet, and A Zettl. Amine-functionalized boron nitride nanotubes. *Solid State Communications*, 142(11):643–646, 2007.
- [61] Albert S Nazarov, Viktor N Demin, Ekaterina D Grayfer, Alexander I Bulavchenko, Aida T Arymbaeva, Hyeon-Jin Shin, Jae-Young Choi, and Vladimir E Fedorov. Functionalization and dispersion of hexagonal boron nitride (h-bn) nanosheets treated with inorganic reagents. *Chemistry—An Asian Journal*, 7(3):554–560, 2012.
- [62] V.E. Fedorov, A.S. Nazarov, and V.N. Demin. Method of producing soluble hexagonal boron nitride, 2013. Russian Patent RU 2478077 C2.
- [63] Amir Pakdel, Yoshio Bando, and Dmitri Golberg. Plasma-assisted interface engineering of boron nitride nanostructure films. *ACS nano*, 8(10):10631–10639, 2014.
- [64] Zhenhua Cui, Andrew J Oyer, A Jaeton Glover,

- Hannes C Schniepp, and Douglas H Adamson. Large scale thermal exfoliation and functionalization of boron nitride. *Small*, 10(12):2352–2355, 2014.
- [65] Lu Hua Li, Jiri Cervenka, Kenji Watanabe, Takashi Taniguchi, and Ying Chen. Strong oxidation resistance of atomically thin boron nitride nanosheets. *ACS nano*, 8(2):1457–1462, 2014.
- [66] E Chigo Anota, H Hernández Cocoltzi, and E Rubio Rosas. Lda approximation based analysis of the adsorption of o3 by boron nitride sheet. *The European Physical Journal D*, 63(2):271–273, 2011.
- [67] K. Nemeth, A. M. Danby, and B. Subramaniam. Synthesis of oxygen and boron trihalogenide functionalized two-dimensional layered materials in pressurized medium, 2017. Patent appl. WO/2017/196738 and US/2019/0134585.
- [68] Toby Sainsbury, Amro Satti, Peter May, Zhiming Wang, Ignatius McGovern, Yurii K Gunko, and Jonathan Coleman. Oxygen radical functionalization of boron nitride nanosheets. *Journal of the American Chemical Society*, 134(45):18758–18771, 2012.
- [69] A. Mofakhami and J.F. Fauvarque. Method of activating boron nitride, 2010. US Patent appl. 2010/0280138A1.
- [70] A. Mofakhami and J.F. Fauvarque. Material for an electrochemical device, 2011. US Patent appl. 2011/0091789A1.
- [71] A. Mofakhami and J.F. Fauvarque. Material for an electrochemical device, 2015. US Patent 9,105,907B2.
- [72] G.P. Rajendran. Surface modified hexagonal boron nitride particles, 2012. US Patent 8258346.
- [73] Wenbo Sheng, Ihsan Amin, Christof Neumann, Renhao Dong, Tao Zhang, Erik Wegener, Wei-Liang Chen, Paul Förster, Hai Quang Tran, Markus Löffler, et al. Polymer brushes: Polymer brushes on hexagonal boron nitride (small 19/2019). *Small*, 15(19):1970099, 2019.
- [74] Toby Sainsbury, Arlene O'Neill, Melissa K Passarelli, Maud Seraffon, Dipak Gohil, Sam Gnaniah, Steve J Spencer, Alasdair Rae, and Jonathan N Coleman. Dibromocarbene functionalization of boron nitride nanosheets: Toward band gap manipulation and nanocomposite applications. *Chemistry of Materials*, 26(24):7039–7050, 2014.
- [75] Yi Lin, Tiffany V Williams, and John W Connell. Soluble, exfoliated hexagonal boron nitride nanosheets. *The Journal of Physical Chemistry Letters*, 1(1):277–283, 2009.
- [76] Dongju Lee, Bin Lee, Kwang Hyun Park, Ho Jin Ryu, Seokwoo Jeon, and Soon Hyung Hong. Scalable exfoliation process for highly soluble boron nitride nanoplatelets by hydroxide-assisted ball milling. *Nano letters*, 15(2):1238–1244, 2015.
- [77] Fan Zhang, Károly Németh, Javier Bareño, Fulya Dogan, Ira D Bloom, and Leon L Shaw. Experimental and theoretical investigations of functionalized boron nitride as electrode materials for li-ion batteries. *RSC Advances*, 6(33):27901–27914, 2016.
- [78] RH Wentorf Jr. Synthesis of the cubic form of boron nitride. *The Journal of Chemical Physics*, 34(3):809–812, 1961.
- [79] Aristides Bakandritsos, Martin Pykal, Piotr Błonski, Petr Jakubec, Demetrios D Chronopoulos, Katerina Polakova, Vasilios Georgakilas, Klara Cepe, Ondrej Tomanec, Vaclav Ranc, Athanasios B. Bourlinos, Radek Zboril, and Michal Otyepka. Cyanographene and graphene acid: emerging derivatives enabling high-yield and selective functionalization of graphene. *ACS nano*, 11(3):2982–2991, 2017.
- [80] Yi Heng Cheong, Muhammad Zafir Mohamad Nasir, Aristides Bakandritsos, Martin Pykal, Petr Jakubec, Radek Zboril, Michal Otyepka, and Martin Pumera. Cyanographene and graphene acid: the functional group of graphene derivative determines the application in electrochemical sensing and capacitors. *ChemElectroChem*, 6(1):229–234, 2019.
- [81] Smita V Talande, Aristides Bakandritsos, Petr Jakubec, Ondřej Malina, Radek Zboril, and Jiří Tuček. Densely functionalized cyanographene bypasses aqueous electrolytes and synthetic limitations toward seamless graphene/ β -feoooh hybrids for supercapacitors. *Advanced Functional Materials*, 29(51):1906998, 2019.
- [82] Hyung Mo Jeong, Jung Woo Lee, Weon Ho Shin, Yoon Jeong Choi, Hyun Joon Shin, Jeung Ku Kang, and Jang Wook Choi. Nitrogen-doped graphene for high-performance ultracapacitors and the importance of nitrogen-doped sites at basal planes. *Nano letters*, 11(6):2472–2477, 2011.
- [83] Satyanarayana Emani, Caihong Liu, Maziar Ashuri, Karan Sahni, Jinpeng Wu, Wanli Yang, Károly Németh, and Leon L Shaw. Li3bn2 as a transition metal free, high capacity cathode for li-ion batteries. *ChemElectroChem*, 6(2):320–325, 2019.
- [84] Toby Sainsbury, Melissa Passarelli, Mira Naftaly, Sam Gnaniah, Steve J Spencer, and Andrew J Pollard. Covalent carbene functionalization of graphene: Toward chemical band-gap manipulation. *ACS applied materials & interfaces*, 8(7):4870–4877, 2016.
- [85] Adila Rani, Seung-Woong Nam, Kyoung-Ah Oh, and Min Park. Electrical conductivity of chemically reduced graphene powders under compression. *Carbon Letters (Carbon Lett.)*, 11(2):90–95, 2010.
- [86] Dana Pantea, Hans Darmstadt, Serge Kaliaguine, and Christian Roy. Electrical conductivity of conductive carbon blacks: influence of surface chemistry and topology. *Applied Surface Science*, 217(1-4):181–193, 2003.
- [87] Syed Atif Pervez, Musa Ali Cambaz, Venkataraman Thangadurai, and Maximilian Fichtner. Interface in solid-state lithium battery: Challenges, progress, and outlook. *ACS applied materials & interfaces*, 11(25):22029–22050, 2019.
- [88] Eric C Mattson, Haihui Pu, Shumao Cui, Marvin A Schofield, Sonny Rhim, Ganhua Lu, Michael J Nasse, Rodney S Ruoff, Michael Weinert, Marija Gajdardziska-Josifovska, et al. Evidence of nanocrystalline semiconducting graphene monoxide during thermal reduction of graphene oxide in vacuum. *ACS nano*, 5(12):9710–9717, 2011.
- [89] Si Zhou and Angelo Bongiorno. Origin of the chemical and kinetic stability of graphene oxide. *Scientific reports*, 3:2484, 2013.
- [90] Didier Devilliers, Michel Vogler, Frederic Lantelme, and Marius Chemla. Mass spectrometric analysis of thermal decomposition products of graphite fluorides and electrogenerated carbonfluorine compounds. *Analytica chimica acta*, 153:69–82, 1983.
- [91] Gianfranco Pacchioni, Livia Giordano, and Matteo Baistrocchi. Charging of metal atoms on ultrathin mgo/mo(100) films. *Phys. Rev. Lett.*, 94:226104, 2005.

- [92] Paolo Giannozzi, Stefano Baroni, Nicola Bonini, Matteo Calandra, Roberto Car, Carlo Cavazzoni, Davide Ceresoli, Guido L Chiarotti, Matteo Cococcioni, Ismaila Dabo, Andrea Dal Corso, Stefano de Gironcoli, Stefano Fabris, Guido Fratesi, Ralph Gebauer, Uwe Gerstmann, Christos Gougoussis, Anton Kokalj, Michele Lazzeri, Layla Martin-Samos, Nicola Marzari, Francesco Mauri, Riccardo Mazzarello, Stefano Paolini, Alfredo Pasquarello, Lorenzo Paulatto, Carlo Sbraccia, Sandro Scandolo, Gabriele Sclauzero, Ari P Seitsonen, Alexander Smogunov, Paolo Umari, and Renata M Wentzcovitch. Quantum espresso: a modular and open-source software project for quantum simulations of materials. *Journal of Physics: Condensed Matter*, 21(39):395502 (19pp), 2009.
- [93] P Giannozzi, O Andreussi, T Brumme, O Bunau, M Buongiorno Nardelli, M Calandra, R Car, C Cavazzoni, D Ceresoli, M Cococcioni, N Colonna, I Carnimeo, A Dal Corso, S de Gironcoli, P Delugas, R A DiStasio Jr, A Ferretti, A Floris, G Fratesi, G Fugallo, R Gebauer, U Gerstmann, F Giustino, T Gorni, J Jia, M Kawamura, H-Y Ko, A Kokalj, E Kkbenli, M Lazzeri, M Marsili, N Marzari, F Mauri, N L Nguyen, H-V Nguyen, A Otero de-la Roza, L Paulatto, S Ponc, D Rocca, R Sabatini, B Santra, M Schlipf, A P Seitsonen, A Smogunov, I Timrov, T Thonhauser, P Umari, N Vast, X Wu, and S Baroni. Advanced capabilities for materials modelling with quantum espresso. *Journal of Physics: Condensed Matter*, 29(46):465901, 2017.
- [94] Károly Németh. Ultrahigh energy density li-ion batteries based on cathodes of 1d metals with-li-n-b-n-repeating units in α -lixbn2 (1 x 3). *The Journal of chemical physics*, 141(5):054711, 2014.
- [95] John P. Perdew, Kieron Burke, and Matthias Ernzerhof. Generalized gradient approximation made simple. *Phys. Rev. Lett.*, 77:3865, 1996.
- [96] John P. Perdew, Adrienn Ruzsinszky, Gábor I. Csonka, O. A. Vydrov, G. E. Scuseria, L. A. Constantin, X. Zhou, and K. Burke. Restoring the density-gradient expansion for exchange in solids and surfaces. *Phys. Rev. Lett.*, 100:136406, 2008.
- [97] Viktor Zolyomi and J Kürti. Towards improved exact exchange functionals relying on g w quasiparticle methods for parametrization. *Physical Review B*, 92(3):035150, 2015.
- [98] John P Perdew, Matthias Ernzerhof, and Kieron Burke. Rationale for mixing exact exchange with density functional approximations. *The Journal of chemical physics*, 105(22):9982–9985, 1996.
- [99] Carlo Adamo and Vincenzo Barone. Toward reliable density functional methods without adjustable parameters: The pbe0 model. *The Journal of chemical physics*, 110(13):6158–6170, 1999.
- [100] Jochen Heyd, Gustavo E Scuseria, and Matthias Ernzerhof. Hybrid functionals based on a screened coulomb potential. *The Journal of chemical physics*, 118(18):8207–8215, 2003.
- [101] Kenji Watanabe, Takashi Taniguchi, and Hisao Kanda. Direct-bandgap properties and evidence for ultraviolet lasing of hexagonal boron nitride single crystal. *Nature materials*, 3(6):404–409, 2004.
- [102] A. Mofakhami and J.F. Fauvarque. Material for an electrochemical device, 2010. US Patent appls. 2010/0280138, 2011/0091789A1, 9105907B2.
- [103] Zhenrong Lu, Li Yang, and Yaju Guo. Thermal behavior and decomposition kinetics of six electrolyte salts by thermal analysis. *Journal of power sources*, 156(2):555–559, 2006.
- [104] SA Polishchuk, LN Ignateva, Yu V Marchenko, and VM Bouznik. Oxyfluoride glasses (a review). *Glass Physics and Chemistry*, 37(1):1–20, 2011.
- [105] Catherine Boussard-Plédel, Marie Le Floch, Gilles Fonteneau, Jacques Lucas, Sourisak Sinbandhit, J Shao, CA Angell, Joël Emery, and JY Buzare. The structure of a boron oxyfluoride glass, an inorganic cross-linked chain polymer. *Journal of non-crystalline solids*, 209(3):247–256, 1997.
- [106] Bala Subramaniam, Daryle Busch, Andrew M. Danby, and Thomas P Binder. Ozonolysis reactions in liquid CO₂ and CO₂-expanded solvents, 2013. US Patent US8801939B2.
- [107] Michael D Lundin, Andrew M Danby, Geoffrey R Akien, Thomas P Binder, Daryle H Busch, and Bala Subramaniam. Liquid co2 as a safe and benign solvent for the ozonolysis of fatty acid methyl esters. *ACS Sustainable Chemistry & Engineering*, 3(12):3307–3314, 2015.
- [108] James D McClure and Paul H Williams. Hydrogen peroxideboron trifluoride etherate, a new oxidizing agent. *The Journal of Organic Chemistry*, 27(1):24–26, 1962.
- [109] Karoly Nemeth. Radical anion functionalization of two-dimensional materials, 2020. Patent appl. PCT/US/20/20383, WO/2020/180680.
- [110] J Stephen Hartman and Jack M Miller. Adducts of the mixed trihalides of boron. In *Advances in Inorganic Chemistry and Radiochemistry*, volume 21, pages 147–177. Elsevier, 1978.
- [111] Louis O. Gilpatrick. Synthesis of sodium hydroxytrifluoroborate, 1974. US Patent 3809762.
- [112] MJR Clark and H Lynton. The crystal and molecular structure of nabf3oh. *Canadian Journal of Chemistry*, 48(3):405–409, 1970.
- [113] Weijiang Zhang, Xiangmei Wang, and Jiao Xu. Kinetic study on preparation of high-purity enriched boric-10 acid used in nuclear power plants. *Asian Journal of Chemistry*, 27(9):3234–3238, 2015.
- [114] Christian A Wamser. Equilibria in the system boron trifluoridewater at 25. *Journal of the American Chemical Society*, 73(1):409–416, 1951.
- [115] WG Paterson and M Onyszchuk. The interaction of boron trifluoride with hydrazine. *Canadian Journal of Chemistry*, 39(5):986–994, 1961.
- [116] Donggun Kim, Xin Liu, Baozhi Yu, Srikanth Mateti, Luke A. O’Dell, Qiangzhou Rong, and Ying (Ian) Chen. Amine-functionalized boron nitride nanosheets: A new functional additive for robust, flexible ion gel electrolyte with high lithium-ion transference number. *Advanced Functional Materials*, 30(15):1910813, 2020.
- [117] Zhizhen Zhang, Hui Li, Kavish Kaup, Laidong Zhou, Pierre-Nicholas Roy, and Linda F Nazar. Targeting superionic conductivity by turning on anion rotation at room temperature in fast ion conductors. *Matter*, 2(6):1667–1684, 2020.
- [118] Won-Sub Yoon, Kwang-Bum Kim, Min-Gyu Kim, Min-Kyu Lee, Hyun-Joon Shin, Jay-Min Lee, Jae-Sung Lee, and Chul-Hyun Yo. Oxygen contribution on li-ion intercalation- deintercalation in licoo2 investigated by o k-edge and co l-edge x-ray absorption spectroscopy. *The Journal of Physical Chemistry B*, 106(10):2526–

- 2532, 2002.
- [119] T Mizokawa, Y Wakisaka, T Sudayama, C Iwai, K Miyoshi, J Takeuchi, H Wadati, DG Hawthorn, TZ Regier, and GA Sawatzky. Role of oxygen holes in Li_xCoO_2 revealed by soft x-ray spectroscopy. *Physical Review Letters*, 111(5):056404, 2013.
 - [120] Dong-Hwa Seo, Jinhyuk Lee, Alexander Urban, Rahul Malik, ShinYoung Kang, and Gerbrand Ceder. The structural and chemical origin of the oxygen redox activity in layered and cation-disordered Li -excess cathode materials. *Nature chemistry*, 8(7):692, 2016.
 - [121] Kun Luo, Matthew R Roberts, Rong Hao, Niccol  Guerini, David M Pickup, Yi-Sheng Liu, Kristina Edstr m, Jinghua Guo, Alan V Chadwick, Laurent C Duda, and Peter G. Bruce. Charge-compensation in 3d-transition-metal-oxide intercalation cathodes through the generation of localized electron holes on oxygen. *Nature Chemistry*, 8(7):684, 2016.
 - [122] Xiaowei Shen, Yutao Li, Tao Qian, Jie Liu, Jinqiu Zhou, Chenglin Yan, and John B Goodenough. Lithium anode stable in air for low-cost fabrication of a dendrite-free lithium battery. *Nature Communications*, 10(1):1–9, 2019.
 - [123] Ying Huang, Bo Chen, Jian Duan, Fei Yang, Tengrui Wang, Zhengfeng Wang, Wenjuan Yang, Chenchen Hu, Wei Luo, and Yunhui Huang. Graphitic carbon nitride ($\text{g-c}_3\text{n}_4$): An interface enabler for solid-state lithium metal batteries. *Angewandte Chemie International Edition*, 59(9):3699–3704, 2020.
 - [124] Zhijin Ju, Jianwei Nai, Yao Wang, Tiefeng Liu, Jianhui Zheng, Huadong Yuan, Ouwei Sheng, Chengbin Jin, Wenkui Zhang, Zhong Jin, et al. Biomacromolecules enabled dendrite-free lithium metal battery and its origin revealed by cryo-electron microscopy. *Nature communications*, 11(1):1–10, 2020.
 - [125] Jiangfeng Qian, Wesley A Henderson, Wu Xu, Priyanka Bhattacharya, Mark Engelhard, Oleg Borodin, and Ji-Guang Zhang. High rate and stable cycling of lithium metal anode. *Nature communications*, 6(1):1–9, 2015.
 - [126] Ilya A Shkrob, Timothy W Marin, Ye Zhu, and Daniel P Abraham. Why bis (fluorosulfonyl) imide is a magic anion for electrochemistry. *The Journal of Physical Chemistry C*, 118(34):19661–19671, 2014.
 - [127] Zhiqiang Xu, Chi kyun Park, Zhiwei Zhang, and Chai Chul. Organic lithium salt electrolytes having enhanced safety for rechargeable batteries and methods of making the same, 2009. US Patent 7534527B2.
 - [128] Kenichi Shinmyo, Tomoe Yoshida, and Masashi Kano. Lithium carboxylate salt-boron trifluoride complex, method for manufacturing the complex, electrolyte solution, method for manufacturing the electrolyte solution, gel electrolyte, and solid electrolyte, 2013. Japanese Patent 2013209355A.
 - [129] Kenichi Shinmyo and Katsu Heiji. Process for producing lithium carboxylic acid salt-boron trifluoride complex, 2017. Japanese Patent 2017178964A.
 - [130] Hongyao Zhou, Sicen Yu, Haodong Liu, and Ping Liu. Protective coatings for lithium metal anodes: Recent progress and future perspectives. *Journal of Power Sources*, 450:227632, 2020.
 - [131] Prices of h-BN , BF_3 and BCl_3 are from www.alibaba.com (various suppliers). Prices of Li , Na and Mg are from price.metal.com (Shanghai Metals Market).
 - [132] Lynn Trahey, Fikile R Brushett, Nitash P Balsara, Gerbrand Ceder, Lei Cheng, Yet-Ming Chiang, Nathan T Hahn, Brian J Ingram, Shelley D Minter, Jeffrey S Moore, et al. Energy storage emerging: A perspective from the joint center for energy storage research. *Proceedings of the National Academy of Sciences*, 117(23):12550–12557, 2020.

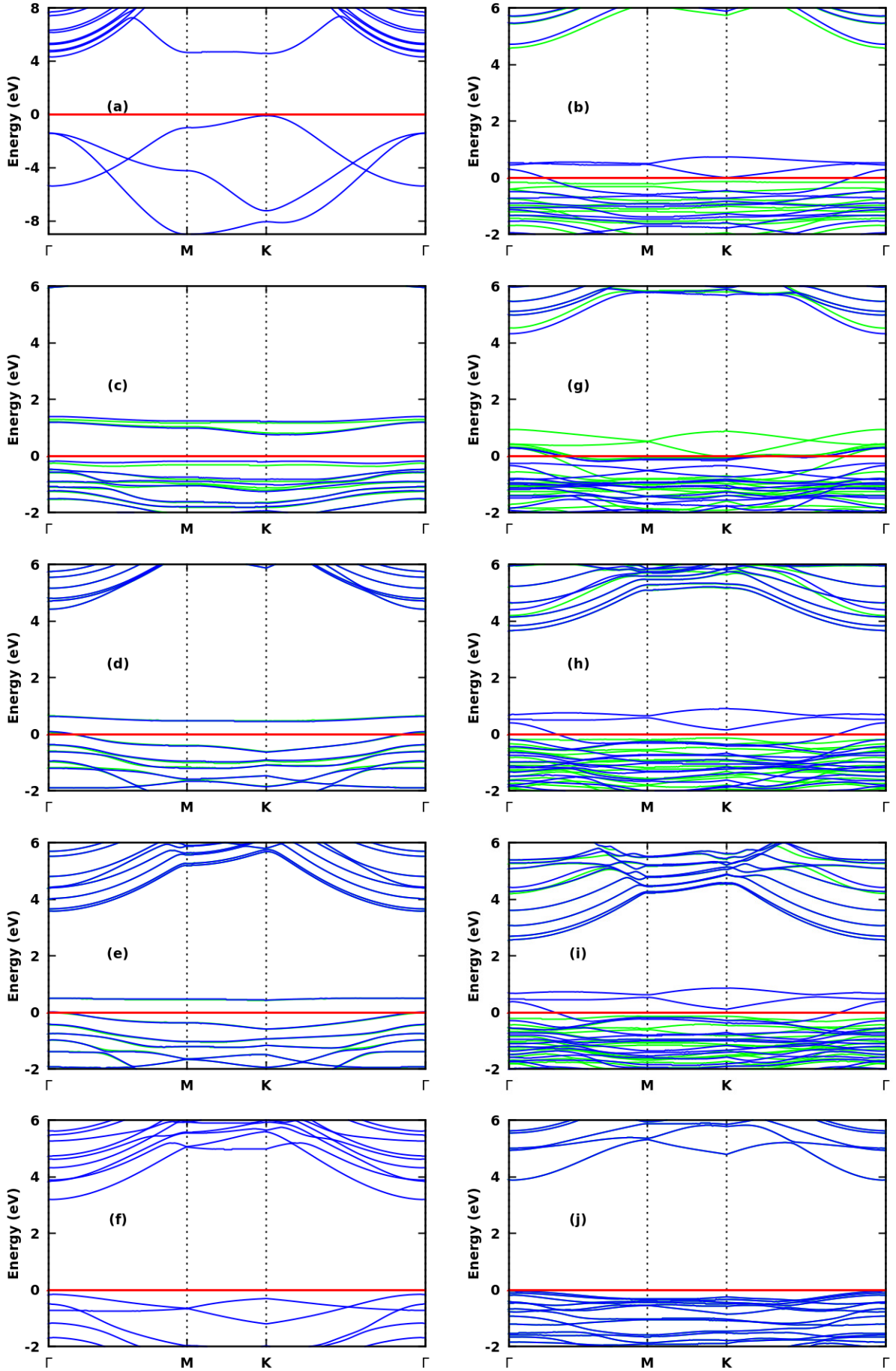


FIG. 3: Band structures of h-BN (a), $(\text{BN})_2\text{OSO}_2\text{F}$ (b), $(\text{BN})_2\text{OBF}_3$ and $(\text{Li/Na/Mg})[(\text{BN})_2\text{OBF}_3]$ (c-f), and $(\text{BN})_2\text{OBCl}_3$ and $(\text{Li/Na/Mg})[(\text{BN})_2\text{OBCl}_3]$ (g-j), respectively. Up and down spin bands are colored differently. Energies are relative to the Fermi energy (red line).